Attosecond spectroscopy of bio-chemically relevant molecules

Calegari, F., Trabattoni, A., Månsson, E., Greenwood, J. B., Decleva, P., Martìn, F., & Nisoli, M. (2018). Attosecond spectroscopy of bio-chemically relevant molecules. *Rivista del Nuovo Cimento*, *41*(8), 415-461. https://doi.org/10.1393/ncr/i2018-10150-2

Published in:
Rivista del Nuovo Cimento

Document Version:
Peer reviewed version

Queen's University Belfast - Research Portal:
Link to publication record in Queen's University Belfast Research Portal

Attosecond spectroscopy of bio-chemically relevant molecules

F. Calegari([1])([2])([3])(*), A. Trabattoni([1]), E. Månsson([1]), J.B. Greenwood([4]), P. Decleva([5]), F. Martìn([6])([7])([8]) and M. Nisoli([9])([3])

([1]) *Center for Free-Electron Laser Science (CFEL), DESY, Hamburg, Germany*
([2]) *Department of Physics, Hamburg Universität, Hamburg, Germany*
([3]) *Institute for Photonics and Nanotechnologies, IFN-CNR, Milano, Italy*
([4]) *School of Maths and Physics, Queen's University Belfast, UK*
([5]) *Dipartimento di Scienze Chimiche e Farmaceutiche, Università di Trieste, Trieste, Italy*
([6]) *Departamento de Qumica, Universidad Autnoma de Madrid, Madrid, Spain*
([7]) *Instituto de Estudios Avanzados en Nanociencia (IMDEA-Nano), Campus de Cantoblanco, 28049 Madrid, Spain*
([8]) *Condensed Matter Physics Center (IFIMAC), Universidad Autonoma de Madrid, 28049 Madrid, Spain*
([9]) *Dipartimento di Fisica, Politecnico di Milano, Milano, Italy*

Summary. — Understanding the role of the electron dynamics in the photochemistry of bio-chemically relevant molecules is key to getting access to the fundamental physical processes leading to damage, mutation and, more generally, to the alteration of the final biological functions. Sudden ionization of a large molecule has been proven to activate a sub-femtosecond charge flow throughout the molecular backbone, purely guided by electronic coherences, which could ultimately affect the photochemical response of the molecule at later times. We can follow this ultrafast charge flow in realtime by exploiting the extreme time resolution provided by attosecond light sources. In this work recent advances in attosecond molecular physics are presented with particular focus on the investigation of bio-relevant molecules.

1. – Introduction

Extreme ultraviolet (XUV) light pulses can induce sudden ionization of a molecule. Once the hole is created, it can migrate along the molecular backbone on a time scale ranging from few-femtoseconds down to hundreds attoseconds [1, 2, 3, 4, 5]. This process has been dubbed charge migration and it is purely driven by the coherent superposition of electronic states generated by the initial pulse. Charge migration can be achieved

(*) francesca.calegari@desy.de

either with inner shell-ionization of highly correlated electronic states or with a broadband pulse, covering several ionization thresholds. In both cases, the process leads to ultrafast charge oscillations until the interplay between the electronic and nuclear degrees of freedom leads to the final localization of the charge on a specific molecular terminus. Charge migration inevitably leads to an ultrafast redistribution of charge, which could ultimately be responsible for the breakage of a chemical bond in the place where the charge has migrated. This concept has triggered the idea of controlling the localization of the charge on an attosecond time scale to induce bond breaking in a specific molecular site, opening the way to the so-called "attochemistry" [6]. Recently, it has been theoretically predicted that even strong non-adiabatic couplings could lead to ultrafast charge transfer (few-femtoseconds) [7], a process competing with charge migration. This occurs when conical intersections are located in proximity of the Frank-Condon region: in this case the nuclear dynamics is expected to affect the light-activated electron dynamics immediately after the ionization.

Photoionization of our own biomolecules activates a number of mechanisms, which need to be investigated at the molecular level. This investigation is key to understanding and ultimately controling the processes leading to damage and mutation of the molecule after irradiation, a critical aspect for the optimization of the radiotherapy treatments. For this reason, considerable effort has been put in the experimental and theoretical investigation of the photo-induced electron dynamics in molecules of increasing complexity. From the experimental point of view, tracing this ultrafast dynamics requires extremely high temporal resolution, such as that provided by attosecond laser sources. XUV attosecond laser pulses can be produced via the high-order harmonic generation (HHG) process and they have been proven to be a valuable tool for real-time tracing of the electron dynamics in atoms, molecules and even solids [8, 9].

In this work we will review the current experimental and theoretical efforts aiming at demonstrating the possibility to exploit attosecond technology to image ultrafast charge dynamics in biologically relevant molecules such as amino acids and DNA nucleobases. We will show that the combination of state-of-the art attosecond techniques with sophisticated theoretical modeling allows valuable information on the complex response of the molecular system to be extracted. The review paper is organized as follows: in Section 2 we will describe the main techniques currently used to generate attosecond pulses in the XUV and soft-X spectral ranges. In Section 3 the application of such ultrashort light transients to molecular science is discussed, with particular focus on small molecules. Section 4 reports on a recent work demonstrating charge migration in aromatic amino acids: this work constitutes the first experimental evidence of XUV induced electron dynamics in bio-relevant molecules. Attosecond spectroscopy of biomolecules using XUV pulses inevitably requires working with gas-phase molecules. In Section 5 we will review some methods that can be used to create intact neutral or charged molecules in the gas phase. Finally, in Section 6 we report on the theoretical advances in describing the molecular dynamics (both electron and nuclear) activated by broadband XUV attosecond pulses in bio-relevant molecules.

2. – Advances in attosecond technology

High-order harmonic generation (HHG) in atoms is the physical process at the heart of the production of attosecond pulses [8, 9]. When an ultrashort pulse is focused in a gaseous medium with intensities larger than $\sim 10^{13}$ W/cm^2, a number of strongly nonlinear effects are produced, which lead to the generation of the high order harmonics

of the fundamental radiation. A train of attosecond pulses are produced, separated by half optical cycle of the fundamental radiation, perfectly synchronized with the driving electric field. The yield is characterized by a broad plateau and by a maximum (cutoff) photon energy given by $\hbar\omega_{max} \approx I_p + 3.17U_p$, where I_p is the ionization potential of the gas and $U_p \propto I\lambda^2$ is the ponderomotive energy, I is the laser peak intensity and λ is the central wavelength of the driving laser pulse. The ponderomotive energy represents the mean kinetic energy of a free electron oscillating in the laser field.

Various techniques have been proposed to confine the generation process to a single event: spectral, temporal and spatial gating techniques have been successfully implemented [10, 11]. The first demonstration of isolated attosecond pulses was achieved by using a spectral gating method, based on the selection of the cutoff spectral region of the broad extreme ultraviolet spectrum obtained by HHG driven by few-optical cycle pulses [12]. The cutoff portion of the XUV spectrum is indeed generated only near the peak of the driving field thus corresponding to light emitted only within one-half of the laser oscillation period. This scheme requires the use of intense sub-5-fs fundamental pulses, with stabilized carrier-envelope phase (CEP). Isolated attosecond pulses with a temporal duration down to 80 as have been generated using this method [13].

2˙1. *Temporal gating for the generation of isolated attosecond pulses.* – The temporal gating schemes are based on the generation of an ultrashort temporal window, where harmonic generation process is allowed: if this window is narrower than the temporal separation between two consecutive attosecond pulses, a single pulse can be obtained. The idea is schematically shown in Fig. 1, in the case of a multi-cycle, one-color driving pulse and in the case of a two-color excitation, obtained by adding a second harmonic field to the infrared (IR) driving pulse. In the second case, if the second harmonic is intense enough the time interval between two consecutive attosecond pulses is increased from one-half to one optical cycle. A widely used temporal gating technique, called po-

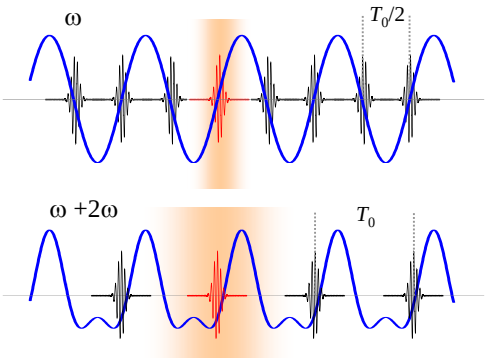

Fig. 1. – Temporal gating: principle of operation in the case of a one- (upper panel) and two-color (lower panel) driving field.

larization gating, is based on the strong dependence of the harmonic generation process on the polarization of the driving radiation. Indeed, the generation efficiency strongly decreases upon increasing the ellipticity of the fundamental field. In 1994 Corkum proposed to generate sub-femtosecond pulses by using a driving pulse with a time-dependent polarization state [14]: circular on the leading and trailing edges and almost linear just around the peak of the pulse, where efficient harmonic generation would be confined.

This idea was experimentally implemented in 2006 [15, 16]: isolated pulses as short as 130 as were generated, consisting of close to a single cycle. The polarization gating technique also requires the use of few-optical cycle driving pulses with stable CEP. By using a two-color excitation obtained by adding the second harmonic to the fundamental frequency (double-optical gating, DOG and generalized DOG, GDOG) it is possible to relax the requirements on the duration of the driving pulse [17, 18, 19].

A different temporal gating method is based on the use of the fast sub-cycle ionization dynamics of the neutral atoms of the gas medium in the presence of an high-intensity IR driving pulse [20]. The key elements of this technique, introduced in 2010, are the following: (i) use of linearly polarized few-optical-cycle driving pulses, with stable CEP and peak intensity beyond the saturation intensity of the gas used for HHG, (ii) optimization of the generation geometry in terms of gas pressure, position and thickness of the gas cell, and (iii) presence of a suitable pinhole for spatial filtering of the generated XUV radiation. Isolated attosecond pulses as short as 155 as were generated, with an energy of a few nanojoules [20].

2˙2. *Light field synthesizer*. – Another powerful technique for the generation of isolated attosecond pulses in the optical region is the so called light field synthesizer, developed by Goulielmakis and coworkers [21, 22]. A coherent supercontinuum was first produced by propagating 22-fs pulses at a central wavelength of 790 nm in a 1.1-m-long hollow fiber filled with neon at a pressure of ~ 2.3 bar [23]. As a result of the propagation inside the hollow fiber the pulse spectrum broadens over more than two optical octaves, ranging from ~ 260 nm to ~ 1100 nm. Temporal compression of the output pulses was obtained by using the technique of coherent combination, or synthesis, of various pulses [24]. The beam at the output of the hollow fiber was divided into four beams by dichroic beamsplitters, characterized by broad spectral bandwidths in four different spectral regions: in the deep ultraviolet, from 270 to 350 nm; in the visible-ultraviolet, from 350 to 500 nm; in the visible, from 500 to 700 nm and in the near IR, from 700 to 1100 nm. The pulses in the four arms of the interferometer were subsequently compressed individually by using chirped mirrors, so that the pulses in the individual channels are compressed close to their bandwidth-limited durations. A pair of thin fused silica wedges was inserted in each channel to finely tune the dispersion and the CEP of the pulses in the different channels. The four pulses were then spatially and temporally superimposed in order to generate a single ultrabroadband pulse. Pulses as short as 380 as were measured [23]. The corresponding electric field and instantaneous intensity profile, measured by using the attosecond streaking technique [25], are shown in Fig. 2.

2˙3. *Attosecond pulses in the soft-X-ray region*. – So far several applications of attosecond pulses have been reported in the XUV spectral region, thus restricting investigations to valence or inner valence electron dynamics. The generation of attosecond pulses in the soft-X-ray (SXR) spectral region gives access to a large number of fundamental processes like ultrafast electronic processes in correlated-electron, magnetic and catalytic materials, charge-induced structural rearrangement [27], change in chemical reactivity [3], photodamage of organic materials [28], ultrafast electron diffraction from within a molecule [29]. Particularly important for the investigation of biological processes is the generation of attosecond pulses in the spectral region between the K-shell absorption edge of carbon (284.2 eV) and the K-edge of oxygen (543.1 eV). Indeed, in this spectral region, called water window, the carbon, oxygen and nitrogen atoms of a cell tissue exhibit a high absorption, while their natural water environment is highly transparent.

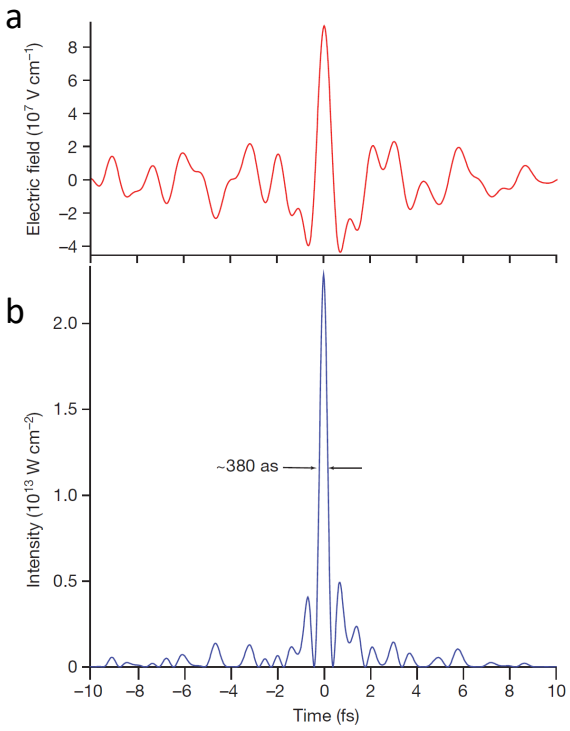

Fig. 2. – Electric field (a) and instantaneous intensity profile (b) of the attosecond pulses generated by the light field synthesizer and characterized by employing the attosecond streaking technique. The intensity profile has a FWHM duration of $\sim$ 380 as. Adapted with permission from Ref. [23].

Since the cutoff energy of the harmonic spectrum scales as λ^2, a natural way to extend the attosecond pulses towards the SXR region is to increase the driving wavelength. The first experimental demonstration of cutoff extension in HHG by using IR pulses at 1.51 μm was reported in 2001 [30]. Since then, many groups have developed high-energy optical parametric amplifiers (OPAs) for HHG [31, 32, 33, 34]. The main disadvantage related to the use of long-wavelength driving radiation is associated to the spatial spreading experienced by the wave packet of the re-colliding electron between tunnel ionization and recombination with the parent ion. This effect leads to a smaller recombination probability and to a lower conversion efficiency: the harmonic yield at constant laser intensity scales as $\lambda^{-6.3\pm1.1}$ in xenon and as $\lambda^{-6.5\pm1.1}$ in krypton over the driving wavelength range of 800-1850 nm [35].

In 2012 bright high-harmonic x-ray supercontinua with photon energies ranging from the XUV to 1.6 keV were produced by focusing 3.9-μm wavelength pulses into a capillary filled with helium at high pressure [26]. This result was obtained on the basis of a careful analysis of the phase-matching conditions for efficient harmonic generation at high-photon energies. Efficient HHG requires macroscopic phase-matching: the driving field and the high-order nonlinear polarization giving rise to harmonic generation have to propagate in phase throughout the medium, thus ensuring a coherent sum of the radiation emitted by many atoms. Phase-matching requires a perfect balance of contributions

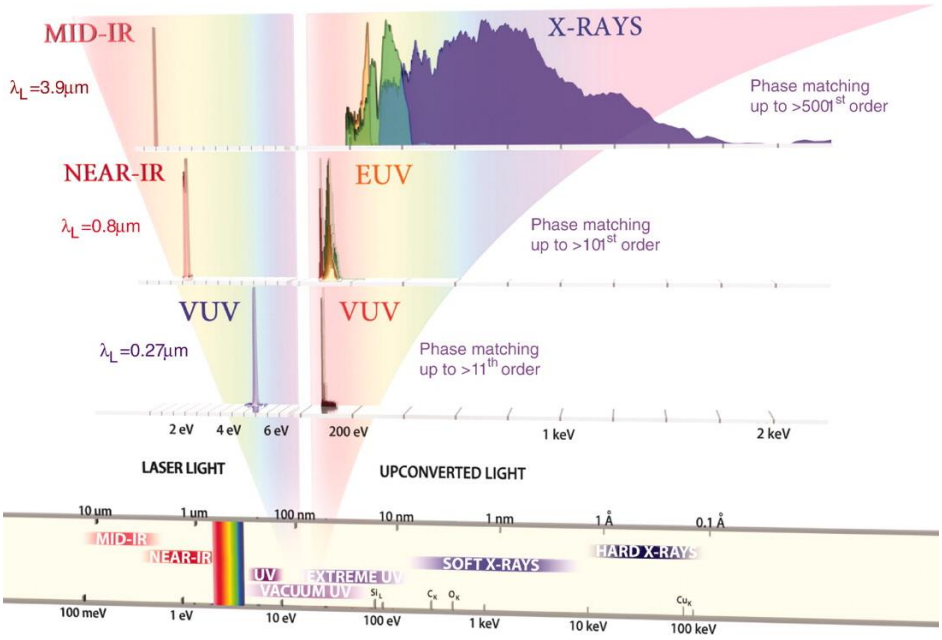

Fig. 3. – Evolution of the harmonic spectra generated in phase-matched conditions, measured by tuning the central wavelength of the driving laser from the ultraviolet ($\lambda_L = 0.27$ μm), to the mid-infrared ($\lambda_L = 3.9$ μm). Adapted with permission from Ref. [26].

from the pressure-dependent neutral atom and free electron dispersions as well as from the pressure-independent geometric dispersion. Experiments and simulations show that the optimal pressure of the gas medium used for HHG increases upon increasing the driving laser wavelength. Figure 3 shows the evolution of the harmonic spectra generated in phase-matched conditions, measured by tuning the central wavelength of the driving laser from the ultraviolet ($\lambda_L = 0.27$ μm), to the mid-infrared ($\lambda_L = 3.9$ μm). The optimal gas pressure ranges from < 0.1 atm in the vacuum ultraviolet (VUV) region to tens of atmospheres in the X-ray region [26]. Moreover, the bright phase-matched HHG spectra evolve from a single harmonic in the XUV into a broad X-ray supercontinuum spanning thousands of harmonics in the soft x-ray region.

Recently, the first streaking measurement of water-window attosecond pulses has been reported [36]. In this case attosecond pulses have been generated by using sub-2-cycle, $1.85-\mu$m laser pulses with stable CEP. The attosecond streaking measurements demonstrated an upper limit of the duration of the isolated pulse of ~ 320 as.

2˙4. *High-energy isolated attosecond pulses.* – Various schemes have been proposed and implemented for the generation of high-energy isolated attosecond pulses [10]. The main target is the possibility to perform attosecond-pump/attosecond-probe experiments, which may typically require peak intensities $> 10^{15}$ W/cm^2. Two proof-of-principle experiments have been reported, based on XUV pump-XUV probe experiments on Xe [37] and H_2 [38]. XUV pulses with energy in the microjoule range can be generated by using the loose-focusing geometry, in which the driving radiation is focused in

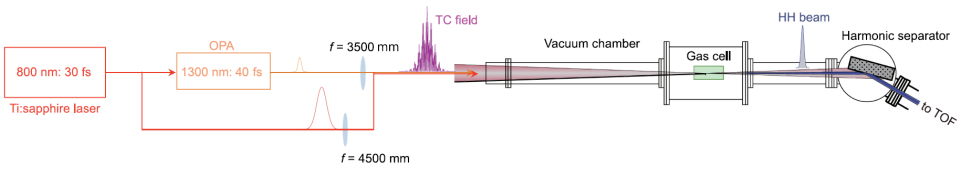

Fig. 4. – Experimental setup for the generation of 1.3 μJ isolated attosecond pulses by using the loose-focusing geometry and a two-color driving pulse. Adapted with permission from Ref. [39].

a long gas cell using a long focal length. In 2013 Takahashi and co-workers reported on the generation of isolated attosecond pulses with a duration of $\sim$ 500 as and an energy up to 1.3 μJ, corresponding to a conversion efficiency of 10^{-4} [39]. The characterization of the attosecond pulses was performed by measuring the second-order autocorrelation in nitrogen. This impressive result was obtained by combining the loose-focusing geometry with the use of a two-color driving pulse. The experimental setup is shown in Fig. 4. Harmonic radiation was generated by using a two-color driving field, obtained by combining in a collinear geometry a 800-nm pulse with an IR pulse at 1.3 μm central wavelength, generated by an optical parametric amplifier (OPA) pumped by a portion of the 800-nm radiation. The xenon target gas was statically filled into the interaction cell of 12 cm length. The two-color technique was employed already in 2009, with the generation of intense XUV continua extending beyond 200 eV by combining an intense few-cycle 800-nm pulse with an IR component [40].

An interesting effect of the use of a two-color driving field is the extension of the cutoff photon energy. If the ratio between the intensities of the IR and 800-nm pulses, $\xi = I_{IR}/I_{800}$, is less than $\sim$ 0.3, the cutoff energy for the two-color driving field is approximately given by [41, 42]:

$$\hbar\omega_{max} \simeq I_p + U_{p0}(3.17 + 1.6\sqrt{\xi}\omega_0/\omega_1) + 3.17U_{p1} \tag{1}$$

where the subscripts 0 and 1 denote the 800-nm and IR pulses, respectively. Equation 1 shows that the cutoff energy can be increased by the supplementary IR field for the same laser intensity.

2˙5. *Attosecond pulses generated by Free Electron Lasers.* – Various schemes have recently been proposed for the generation of ultrashort pulses by using Free Electron Lasers (FELs), in order to increase by orders of magnitude the photon flux [43]. Many of these schemes are based on the use of few-optical-cycle laser pulses to modulate the electron energy or trajectory in a small section of the bunch [44]. The shortest pulse duration which can be achieved by using a FEL is limited by the FEL cooperation length, $\ell_c = \lambda_r/4\pi\sqrt{3}\rho$, where λ_r is the radiation wavelength and ρ is the FEL parameter [45]. ρ is typically on the order of $\sim 10^{-3} - 10^{-4}$ in high-energy FELs. Therefore, in the case of 1.25-nm radiation, the shortest pulse duration supported by the FEL is of the order of $\ell_c/c \simeq 200$ as. In general, the length of typical electron bunches in a FEL is longer than the cooperation length, so that the pulse duration of the generated X-ray pulses is typically on the order of tens of femtoseconds as limited by the electron bunch length [43].

Here we cite a single experimental result achieved at the Linac Coherent Light Source by Helm and co-workers [46]. The FEL pulse duration was directly measured by using a single-shot implementation of near-infrared streaking spectroscopy. The experimental scheme is independent of photon energy and it is decoupled from machine parameters. An average duration of 4.4 fs was measured for the FEL pulses. Moreover, an analysis of the pulse substructure has demonstrated the generation of a small percentage of the FEL pulses consisting of individual high-intensity spikes with a duration of the order of hundreds of attoseconds, in good agreement with theoretical predictions. This is a particularly important result, paving the way to the generation of attosecond pulses from a FEL on a reproducible basis.

3. – Attosecond spectroscopy of molecules

The typical time scale of structural changes in molecular systems ranges from picoseconds to femtoseconds. The temporal evolution of electronic wavepackets in molecules, instead, is expected to occur on a sub-femtosecond time scale. Advances in attosecond technology (described in Section 1) have provided unique tools to track in real time ultrafast electron dynamics induced in gas-phase molecules[6]. A typical attosecond experiment is based on the combination of XUV isolated attosecond pulses or attosecond pulse trains with femtosecond NIR pulses. In the following, we will revise the main advances in attosecond molecular spectroscopy based on this time resolved scheme (XUV pump -NIR probe) combined with the detection of charged photofragments or transient XUV spectra. Isolated attosecond pulses have been used together with waveform-controlled ultrashort NIR pulses to control charge localization after sudden ionization of H_2 (D_2) molecules[47]. More recently, the photoionization of N_2 by isolated attosecond pulses has been investigated with extremely high temporal resolution, by measuring the time-resolved momentum distribution of the charged particles created after the interaction. As a result, a deep understanding of the dissociative dynamics together with crucial information on the shape of the potential energy curves involved in the dissociative process have been retrieved[48]. Molecular nitrogen has also been used as a target for an attosecond transient absorption (ATA) spectroscopy experiment[49]. In this work, a new understanding about bound Rydberg and valence states below the first ionization potential was achieved. Attosecond technology has been also exploited to investigate the ionization dynamics in camphor molecules, providing a new insight of the interaction between light and chiral molecules and representing an excellent example of attosecond spectroscopy of molecular systems of increasing complexity[50].

The first pump-probe experiment in molecules with attosecond time resolution was perfomed in 2010 by Sansone et al.[47]. Isolated XUV attosecond pulses, with a duration around 400 as and an energy range between 20 and 40 eV, were used in combination with 6 fs, carrier-envelope-phase-stable NIR probe pulses to investigate the photo-induced electron dynamics following the photoionization of hydrogen (H_2) and deuterium (D_2) molecules. The attosecond pulse was exploited to suddenly ionize the molecules. Then, the angle-resolved momentum distribution of the produced H^+ and D^+ fragments was collected and measured in a velocity map imaging spectrometer (VMI) as a function of the delay between the isolated attosecond pulse and the NIR pulse. In particular, electron localization has been identified by measuring the difference in the yield of H^+ and D^+ ions arriving on the left-hand and right-hand sides of the detector. This asymmetry parameter showed sub-cycle oscillations as a function of the delay between the XUV and

the NIR pulses, in the kinetic energy range between 2 and 10 eV. The measured asymmetry was interpreted as a clear indication of electron localization resulting from the coherent superposition of gerade and ungerade states of the molecule. The experiment demonstrated that electron localization, following XUV-induced dissociative ionization of hydrogen, can be induced by the presence of an external NIR field. In particular, the localization arises from two different mechanisms, where the probe NIR pulse acts on the photoionization of the molecule or on the dissociation of the molecular ion. In the first case, charge localization results from quantum interference involving autoionizing states and the laser-dressed wavefunction of the outgoing electron. In the second case, charge localization is initiated by laser-induced population transfer between different electronic states of the molecular ion. This pioneering result demonstrated for the first time the possibility to exploit attosecond technology to gain access to the electron dynamics in a molecule.

One year after this experiment, the same molecule was investigated by Kelkensberg et al. using a similar approach. Nevertheless, for this experiment an XUV attosecond pulse train was combined with a relatively long NIR pulse with moderate peak intensity ($3 \cdot 10^{13}$ W/cm^{-2}). Compared to the previously described experiment, where isolated attosecond pulses were used to initiate the electron dynamics subsequently probed by the NIR field, in this case the attosecond pulse train was used to photoionize molecular hydrogen in the co-presence of the NIR pulse in order to selectively excite specific electronic states [51].

Following these pioneering experiments performed in the simplest molecule, namely hydrogen, many works have been conducted to explore the intrinsic nature of the electronic motion and to investigate the dissociative dynamics in molecules of increasing complexity. In 2011, Siu and coworkers demonstrated the possibility of controlling O_2^+ dissociation again by using the combination of an XUV pulse train and a long NIR pulse. In this work, the NIR probe pulse was used to control the couplings between different electronic states in the molecular ion after XUV photoionization[52]. Few years later, Cörlin et al. investigated the photodissociation of the same molecule by detecting charged fragments and photoelectrons in coincidence using a reaction microscope. In this case, the attosecond resolution provided by the experiment has been crucial to achieve a new understanding of the vibrational motion occurring in the binding potential of the parent ion O_2^+, as well as to gain a deeper insight into the potential energy curves involved in the ultrafast process[53]. Other important results were obtained in the same period, achieving an unprecedented knowledge of photo-induced ultrafast processes occurring in multi-electron diatomic and small polyatomic molecules[54, 55].

Among these works, it is worth mentioning the extensive studies on ultrafast dissociative ionization of molecular nitrogen induced by attosecond pulses. Molecular nitrogen is the most abundant species in the Earth's atmosphere, and the investigation of the electron dynamics following the absorption of high-energy photons represents a unique tool to better understand the origin of many radiative-transfer processes occurring in the upper layers of the planetary athmospheres. In this perspective, Eckstein et al. recently investigated the dissociative ionization of molecular nitrogen at selected XUV photon energies using a table-top XUV time-compensated monochromator [56]. In this work, the photoionization induced by monochromatic XUV pulses has been probed by time delayed NIR pulses with the detection of charged photoions and photoelectrons. As a

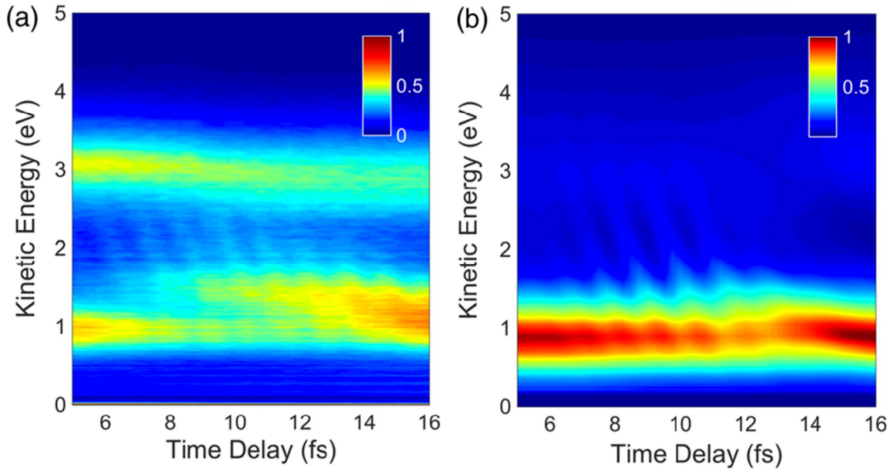

Fig. 5. – Time-dependent N^+ kinetic energy spectra acquired within the pump-probe delay interval 5-16 fs.(b) Simulation of time- dependent N^+ kinetic energy spectra in the same delay interval. Reprinted with permission from Ref. [48]

result, the main dissociation channels resulting from inner-valence ionization have been assigned, which could be influential for modelling of atmospheric chemistry [57].

One of the most important challenges in attosecond spectroscopy is extrapolating results from the broadband excitation intrinsically associated to such extremely short light transients. As mentioned above, a prototypical attosecond excitation inevitably leads to the superposition of a large number of electronic states in the target and the interpretation of the experimental results in this regime of excitation is already an extreme challenge for small molecules. Therefore, theoretical models including a precise description of the potential energy curves and couplings between all the electronic states represent a crucial tool to guide the experimental results.

Recently, Trabattoni et al [48] investigated the dissociative ionization dynamics of molecular nitrogen with extremely high temporal resolution by exploiting a combination of state-of-art attosecond technology and a sophisticated theoretical model. In this way it has been possible to access precise information on the shape of the potential energy curves involved in the dissociative mechanism. In the experiment, an ensemble of nitrogen molecules was photoionized by a sub-300-as attosecond pump pulse in the energy range between 16 and 50 eV, in combination with a waveform-controlled sub-4 fs NIR probe pulse. The angle-resolved momentum distribution of the N^+ fragments was measured with a velocity map imaging spectrometer as a function of the delay between the attosecond pump pulse and the NIR probe pulse. Figure 5(a) shows the delay-dependent kinetic energy spectrum of N^+, obtained by integration of the angular distribution over a small angle along the laser polarization axis. In the figure a pump-probe delay range between 5 and 16 fs is reported. Two main features can be observed in the pump-probe map: (i) the depletion of the signal at 1 eV occurring around 8 fs after the zero delay,

(ii) the appearance of a fringe pattern in the same delay range, with a periodicity of 1.22 fs. Furthermore the modulation shows an energy-dependent phase, resulting in a tilt of

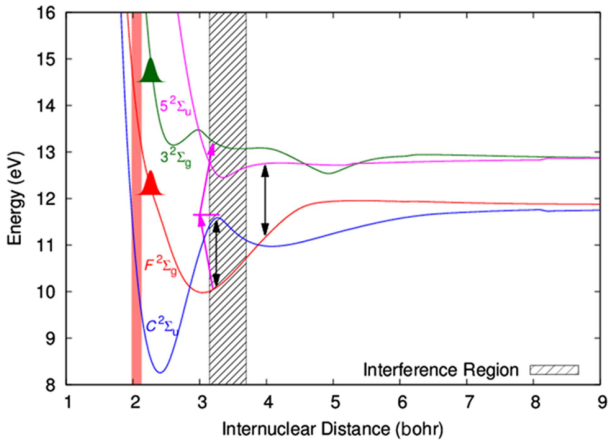

Fig. 6. – Four-state model, where the $F^2\Sigma_g$, $3^2\Sigma_g$, $C^2\Sigma_u$ and $5^2\Sigma_u$ are considered. Reprinted with permission from Ref. [48].

the fringes. In order to unravel the intricate experimental observations, a sophisticated theoretical model was developed. The time-dependent Schrödinger equation (TDSE) has been solved for a set of 616 diabatic excited states of N_2^+, where all the couplings induced by the NIR probe pulse between the states were considered. Then, the TDSE was solved by using a split-operator technique in combination with fast-Fourier techniques. In this approach, the nuclear wave packet (NWP) is discretized on a grid of internuclear distances and the propagation of the wave packet is performed on a set of coupled diabatic electronic states calculated on the same grid. Figure 5(b) shows the numerical calculation of the delay-dependent kinetic energy of the N^+ fragments, simulating the experimental parameters. As can be seen from this figure, the numerical results are in a very good agreement with the experimental ones in the energy region 0-2.5 eV. As a side effect of such a precise numerical calculation, the physical interpretation of the ultrafast process occurring in the molecular ion remains unclear, as well as the specific potential energy curves involved in the dynamics. For this reason, a simplified model was introduced, for which only four states were considered, namely the $F^2\Sigma_g$, $3^2\Sigma_g$, $C^2\Sigma_u$ and $5^2\Sigma_u$ states. This simplified model was able to reproduce the main features observed in the experiment. It also allows one to unravel the physics occurring in the molecule, as schematically represented in figure 6: the depletion of the signal around 1 eV is a consequence of resonant single-photon transitions from the $F^2\Sigma_g$ state to the $5^2\Sigma_u$ state and from the $F^2\Sigma_g$ state to the $C^2\Sigma_u$ state induced by the NIR probe pulse (black double- headed arrows in the figure). The measured delay of 8 fs for the depletion corresponds to the time required by the NWP to reach the single-photon transition point, where the couplings between the states listed above is strong enough to efficiently induce population transfer. Additionally, the ultrafast periodic modulation observed on top of the depletion results from the interference between the initial population of the $3^2\Sigma_g$ state and the population transferred to the $3^2\Sigma_g$ state from the $F^2\Sigma_g$ state via a two-photon transition, where the $5^2\Sigma_u$ state is exploited as a virtual intermediate state

(magenta single-headed arrows). The tilt in the fringes can be easily interpreted as a consequence of the dispersion accumulated by the components of the NWP along the potential energy curves. From this time-versus-energy dependence one can extract precise information about the quantum path followed by the nuclear wave packet, namely the shape of the potential energy curves involved in the interference. By artificially altering the slope of the $3^2\Sigma_g$ state in the simulation, the resulting tilt in the fringes is dramatically affected and it is no longer in agreement with the experimental data. In addition, the sophisticated model developed here provided accurate values for the dissociative ionization yields. It revealed that realistic modelling of the nitrogen photochemistry should also incorporate large amounts of nitrogen atoms or ions in various excited states, which are expected to have a different reactivity.

The experiments described above investigated the photoinduced electron dynamics occurring in molecules by measuring the angle-resolved momentum distribution and the time-dependent yield of the charge particles (ions or electrons) created on target. Similar results can be obtained by using all-optical techniques that do not require the detection charged particles. Among these, attosecond transient absorption (ATA) spectroscopy is a powerful method to access novel ultrafast dynamics occurring in the highly excited states of atoms and molecules[58].
In a prototypical ATA experiment, an attosecond pulse train or an isolated attosecond pulse is transmitted through a target, for example a high-density gaseous ensemble or a thin-film sample. Here the attosecond pulse excites a coherent superposition of dipole-allowed electronic excited states, that corresponds to a time-dependent charge distribution in the target. This photoinduced polarization in the target is responsible for the emission of photons that interfere with the incident XUV field, resulting in novel features in the absorption spectrum of the attosecond pulses. The absorption spectrum in the spectral range covered by the attosecond pulses is measured by an XUV spectrometer. As in the most conventional approach for attosecond spectroscopy, the attosecond pump pulse is combined with a femtosecond NIR probe pulse. This NIR pulse modifies the photo-induced polarization of the target by ionizing or coupling adjacent electronic states. The measurement of the XUV absorption spectrum as a function of the pump probe delay is the main observable of this technique. ATA spectroscopy provides an excellent tool to achieve time and energy resolution at the same time. The temporal resolution is defined by the duration of the pump and the probe pulses and by the stability in the relative delay, while the energy resolution is defined by the resolution of the XUV spectrometer. In the last few years, ATA spectroscopy was widely used to explore ultrafast dynamics in atoms. The temporal evolution of electronic Rydberg wavepackets was observed[59, 60, 61], as well as the creation of transient light-induced states[62, 63]. In 2014, Ott and coworkers demonstrated the ability of retrieving the correlated two electron dynamics occurring in helium[64]. Recent works have extended this technique to small molecular systems, demonstrating the ability of ATA experiments to reach a new understanding of ultrafast electronic processes occurring in molecules. In particular, Reduzzi et al. were able to measure the lifetime of autoionizing Rydberg states in molecular nitrogen, and to track a number of quantum beatings between electronic states. The amplitude of the quantum beats was even controlled by a proper shaping of the initial wavepacket created by the attosecond pulses[65].
More recently, ATA has been used to measure oscillatory dynamics in N_2 after creation of a wavepacket including both bound Rydberg states and valence electronic states [49]. In this work a coherent superposition of bound electronic states was prepared in the

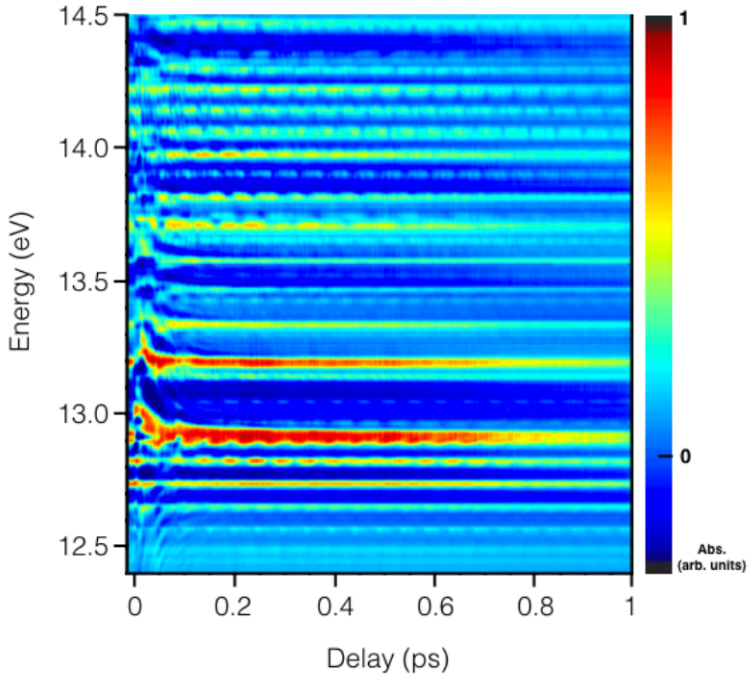

Fig. 7. – The delay dependent absorption of nitrogen for time delays out to 1 ps shown in the 12.4-14.5 eV energy range. The color scale represents absorption. Adapted from Ref. [49]

molecule by an isolated attosecond pulse. To do this end, the spectrum of the attosecond pulse was properly filtered in order to cover the energy region between 12 and 17 eV. Then, a delayed 6-fs NIR pulse was used to modify the structure of the wavepacket by coupling adjacent electronic states. Fig.7 reports the delay-dependent absorption spectrum. As can be observed in the figure, the ATA spectra showed clear oscillations with a period of 50 fs, which has been assigned to the vibrational dynamics in a valence state. The oscillations observed in individual vibrational levels allow one to access the anharmonicity of the potential well and allows the interplay between valence vibrational levels and Rydberg vibrational levels to be identified. A simple model developed within the framework of the Born-Oppenheimer-approximation was introduced in order to describe the possible quantum pathways induced by the probe pulse between adjacent states. The NIR induced couplings are acting as a filter for the electronic excitation, drastically reducing the number of states contributing to the observed quantum beats. Indeed, a simplified model considering only 12 electronic states was able to well reproduce the bound state dynamics of the nuclear wavepacket. This experiment represents an important example of ATA spectroscopy applied to simple molecules and opens the perspective for achieving a deep understanding of ultrafast non-adiabatic dynamics in more complex molecular systems.

It is worth mentioning that Beaulieu et al. recently performed an experiment of self-referenced attosecond photoelectron interferometry, where circularly polarized UV and NIR photons were exploited to drive photoionization of chiral molecules[50]. In particular, by using a superposition of 400-nm and 800-nm laser pulses they were able to measure asymmetric delays in the electron photo-emission from camphor molecules, on both femtosecond and attosecond time scales. This novel approach of attosecond spectroscopy allows for attosecond quantum control and for a better understanding of the chiral interaction with light.

Attosecond photoelectron spectroscopy has been recognized to be sensitive to the electron scattering phase, or, more precisely, to its energy derivative, known as the Wigner-Smith delay. Recently, Huppert et al. demonstrated that attosecond interferometry, based on the use of an XUV attosecond pulse train and a synchronized infrared pulse, can be successfully transposed to small triatomic molecules in both gas and liquid phase [66]. Energy-dependent photoionisation delays have been retrieved for both N_2O and H_2O in the photon-energy range between 20 eV and 40 eV. The remarkable energy dependence of the delays measured in in the case of N_2O has been assigned to the presence of shape resonances, while the smooth decrease in delays measured as a function of the photon energy for H_2O has been found to simply reflects the energy dependence of the Coulomb phase shifts.

In summary, the experiments described in this section demonstrates the ability of attosecond spectroscopy to track ultrafast electron and nuclear dynamics in molecules with increasing complexity. The presented works have paved the way to a new class of experiments aimed at investigating the role of the electron and nuclear dynamics in the photochemistry of bio-chemically relevant molecules.

4. – Charge migration in bio-relevant molecules

An essential part of the molecular processes in life is the control and transfer of electrical charge within large molecules. *Charge transfer* can occur in several ways and on different timescales, and this review will focus on the limiting case of *charge migration* which has been defined as changes in electron density without significant nuclear motion[67, 68, 5]. In line with the Born–Oppenheimer approximation, factorizing the total wavefunction into separate wavefunctions for the electronic and the nuclear/vibrational coordinates, it is theoretically attractive to be able to study fast changes in electron density while keeping the molecular backbone fixed. The validity of such an approximation and the ways in which nuclear motion eventually leads to "decoherence" or blurring of short-time charge density oscillations is currently an active area of theoretical research[69, 70]. At the same time, the first time-resolved measurements of oscillations due to pure charge migration have been reported with attosecond methods.

Photoionization of an isolated molecule by a coherent broadband pulse excites a superposition of molecular orbitals at different energies, leading to a beating/oscillation in the total probability amplitude for the localization of the electron-hole within the molecule. Depending on the energy separation of the contributing states, the observable oscillation can be predicted to have periods of a few femtoseconds to hundreds of attoseconds[71, 68]. A superposition of different electronic states can also be created without requiring a broadband pulse, due to intrinsic electron–electron correlation effects in the molecule (final-state correlation). This kind of excitation can be simulated without

assuming a specific pulse shape and if the initial hole is localized at a particular site of the molecule it is natural to expect a distinct migration of this hole to be observable. To prepare such a hole tends to require high photon energies, to remove an electron from a core or inner orbital (possibly also resulting in double ionization) [5, 7, 72, 73]. Since pump–probe resolution below 10 fs is not yet available with x-ray free electron lasers[74] the temporal observations of charge migration to date were obtained with attosecond pulses in the XUV spectral region. Charge migration in polyatomic molecules has been part of several recent reviews, with emphasis on theory[70] or experiment[11, 68].

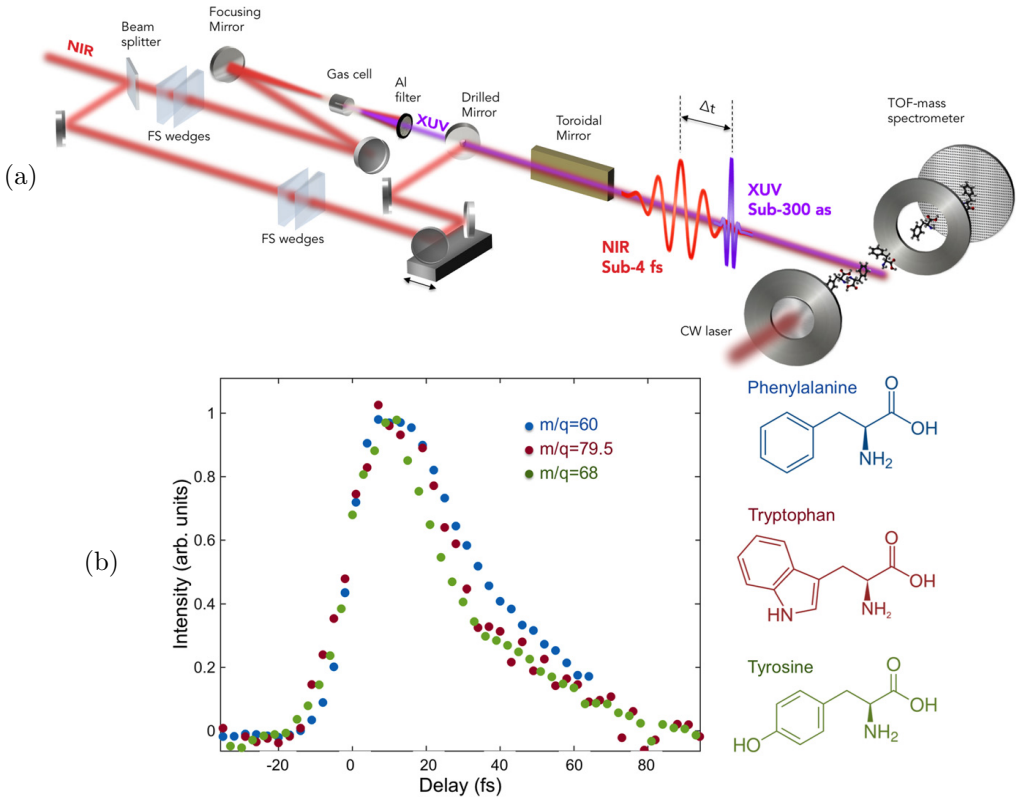

Fig. 8. – Attosecond XUV pump – NIR probe experiments in aromatic amino acids. The lower panel shows the yield of doubly charged immonium-type ions, i.e. the result of additional ionization by the probe pulse and loss of the carboxyl (COOH) group. Reprinted with permission from Ref. [11].

Photolyase proteins are biological systems where the intricate electron transport mechanisms have been widely investigated, following near-UV photoexcitation this mechanism aids repairing the photo-damaged DNA. In this class of proteins, there is a sequence of aromatic amino acids whose role in the charge transfer was recently examined through simulations[76]. Aromatic amino acids such as tryptophan, tyrosine and phenylalanine are indeed considered the nano-sized antenna of proteins as they can capture light very efficiently. For these reason they have been investigated also with attosecond methods, which led to the first time-resolved evidence of charge migration in a biologically relevant molecule[71]. We will here summarize the key point of those experiments.

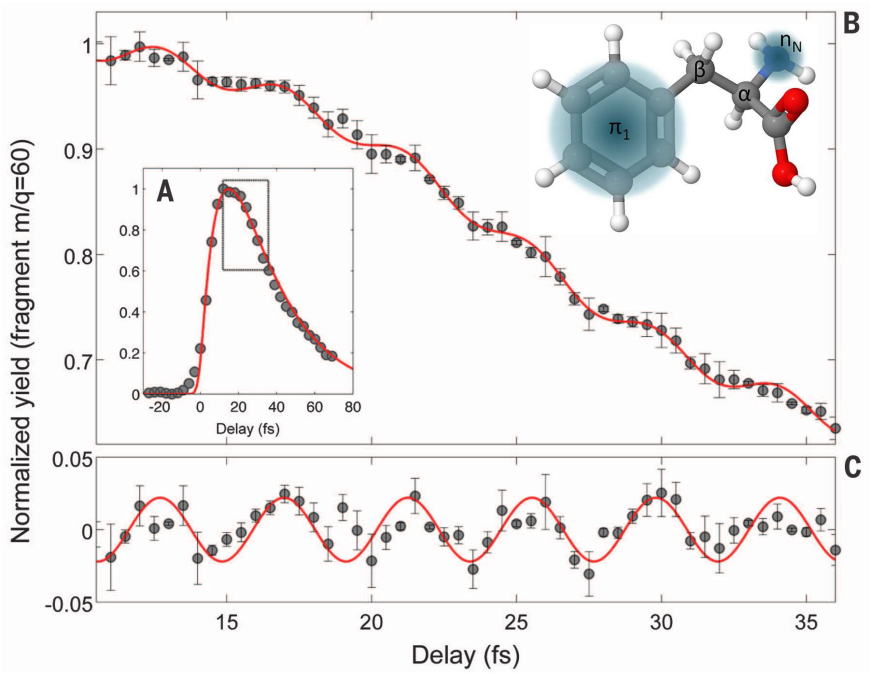

Fig. 9. – The doubly charged immonium yield from phenylalanine, with better time resolution, and the residual oscillation after subtracting the smoothed step function. Figure from [71, Fig. 2] with the molecular structure inset from [75] which indicates the two highest-energy molecular orbitals (n_N at the amine-nitrogen and π_1 at the phenyl group).

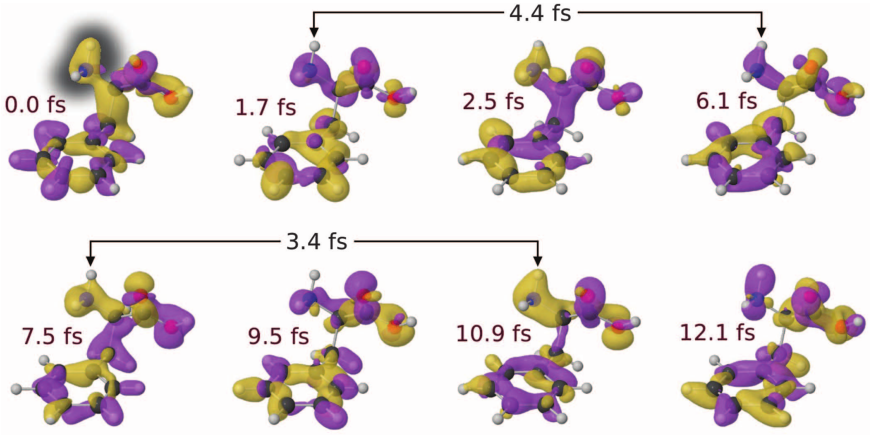

Fig. 10. – Simulated variation in hole density on phenylalanine (+ in yellow, − in blue) after exposure to an isolated attosecond pulse. Reprinted with permission from Ref. [71].

Figure 8(a) gives an overview of the experimental set-up, where a a few-cycle near-infrared (NIR) laser pulse is split into one beam for generation of attosecond pulses and one beam for use as a probe at an adjustable delay. Attosecond pulses in the XUV region are generated with a spectrum extending from 15–16 eV to 35–40 eV, after polarization gating and passage through an aluminium filter. In the first set of experiments with the three amino acids shown in Figure 8(b), XUV pulses of 1.5 fs (and NIR pulses of 6 fs) duration were used in order to maximise the photon flux [75], while the subsequent experiment in phenylalanine used isolated attosecond pulses shorter than 300 as (and NIR pulses of 4.5 fs) to achieve the best time resolution[11]. The samples were transferred to the interaction region of a mass spectrometer at first by laser-induced acoustic desorption (LIAD) [75] and afterwards by simple laser-induced evaporation [11]. Mass spectra of the produced ions were recorded as function of the pump–probe delay. Details about the production of biomolecules in the gas phase will be provided in Section 6. Each amino acid can produce a doubly charged immonium-type ion after double ionization and loss of the carboxyl COOH group, and as seen in Figure 8(b) these fragments demonstrate a strong time dependence. The probing pulse is not able to create doubly charged immonium ions at negative delays, before XUV-photoionization has occurred. At positive delays the yield of the doubly charged fragments decrease with lifetimes of 20–25 fs, which demonstrates that an ultrafast relaxation has occurred, depleting the state produced by XUV-photoionization. Such a time scale is compatible with prompt motion of the nuclei away from the Franck–Condon region on steep potential energy gradients of the excited state.

In phenylalanine, the follow-up experiment with improved time resolution revealed a few-femtosecond periodic modulation overlaid on the smooth step function of the yield of doubly charged immonium, as can be seen in Figure 9. The yield turned out to be oscillating with a period of 4.3 fs, which does not correspond to the single optical cycle ($\sim$ 2.6 fs) of the probing NIR pulse and it is well below the shortest vibrational mode of phenylalanine (9 fs period). Extensive theoretical simulations (more details are provided in Section 7), using the spectrum of the actual XUV pulse to ionize and excite a superposition of 32 states, but neglecting the probing NIR field, allowed the beating of the ion yield to be identified as mainly representing periodic electron density charge fluctuations around the amine group (top, right region of the molecule in Figure 9) [71].

It is worth mentioning that the pure electron dynamics indicated as charge migration is not the only process predicted to occur immediately after sudden ionization. Recently, a theoretical prediction of sudden charge transfer was indeed made for glycine when starting from a localized core-hole (oxygen $2s^{-2}$, representing Auger double ionization): Figure 11(a) shows, by charge densities, that one of the holes is completely transferred to the nitrogen atom at the other end of the molecule within 4 fs although this also involves bond length changes of 0.3 Å[7]. A few femtoseconds later the hole is partially returned and diffused. As a result of strong non-adiabatic couplings the charge can be driven from one molecular site to another on a very fast time scale, competing with the charge migration process.

It may be worth noting that there is no strict definition of how much nuclear motion should be tolerated within the classification of molecular dynamics as charge migration. Although the transfer of a proton to a different site[77, 78] would not qualify, less dramatic coordinate changes typically play a role in defining a reaction path through the potential energy landscape of the electronic states (e.g. by conical intersections) and according to recent theoretical work this may occur even in a few femtoseconds[7, 79]. Experimentally,

it is still possible to distinguish a new paradigm of electron-centered time-resolved studies of molecules enabled by attosecond and few-femtosecond light sources. Nuclear motion on longer timescales has been studied on the picosecond and multi-femtosecond timescales with pump–probe schemes for some time now, using ionization [80, 81] or spectrally resolved absorption [82, 83, 84]. The latter method, known as 2D electronic absorption spectroscopy can trace population changes in spectrally distinct bound states, which can reveal charge migration/transfer when the chromophores are located in different parts of a molecule. Somewhat analogously, as detailed also in Section 3, attosecond methods can be grouped into those probing by ionization (detecting the ions and/or electrons) and those probing by transient absorption[85, 73], both with the promise of tracing the electronic origin of photochemical reactions.

Typically, a photoionized or excited molecule is no longer at an equilibrium geometry. Nuclear motion is thus induced in the form of vibrational modes or Coulomb explosion. Although nuclear motion can be considered as a coherent wavepacket, the fact that we have a superposition of electronic states complicates the picture. Initial electronic oscillations are expected to be washed out as the nuclear coordinates change, which tends to shift the eigen-frequencies of the electronic states rather arbitrarily and presumably prevent a well-defined beating frequency from remaining. However, observable electronic oscillations can be sustained for more some 10 or 20 fs in particular cases where multiple electronic states have parallel potential energy curves/surfaces.[69, 70]. A more detailed discussion on the theoretical description of the effects of nuclear dynamics on the electronic coherences is discussed in Section 7.

Migration of electron/hole density from a donor site to an acceptor site, without long-range motion of nuclei, can still be observed after decoherence if the associated

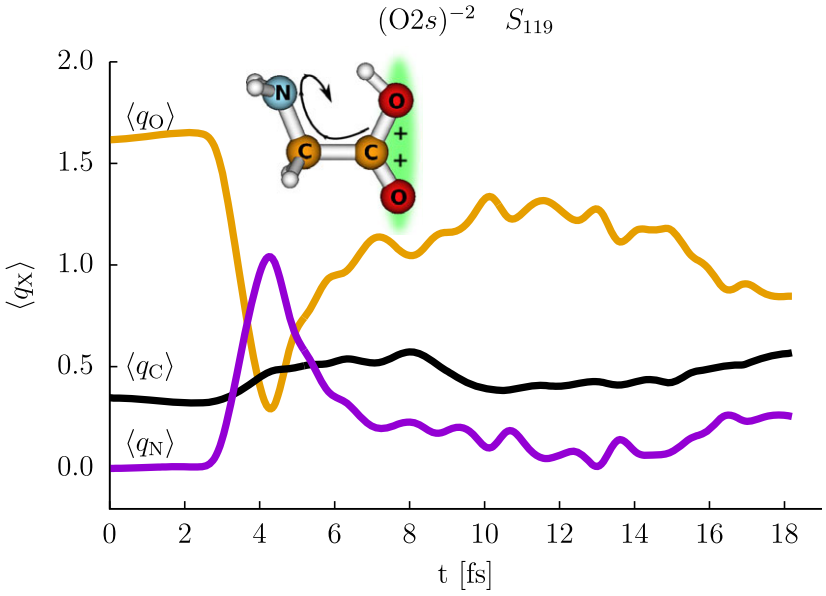

Fig. 11. – Charge density in different parts of glycine molecule when starting from a double hole localized at the oxygen side $2s^{-2}$, but appearing on the nitrogen side at 4 fs. Reprinted with permission from Ref. [7].

(localized/chromophore) states have spectrally different signatures. This type of process is of great interest in molecules involved in biological photoreactions such as vision and photosynthesis, of which many studies have been made using 2D electronic absorption spectroscopy [82, 83, 84] whereby the population of distinct electronic states is followed through spectrally resolved absorption and stimulated emission measurements, using two or more laser pulses. The state-population changes observed lie on the scale of hundreds of femtoseconds or more, with detailed information coming from the spectral resolution.

5. – Ultrafast spectroscopy of DNA subunits

Another class of biologically relevant molecules that has consistently shown very fast decays of the excited state are the sub-units of DNA/RNA. There is a particularly strong interest in the dynamics of excited DNA and RNA, for multiple reasons:

- It has an essential role as information carrier in biology, with applications in medicine and possibly other types of molecular machines.
- Yet, the nucleobases strongly absorb UV radiation which leads to excitations with the potential to disrupt the genetic information. What are the mechanisms that allow this energy to be dissipated without unacceptable rates of mutations? What role did UV absorption play in the initial stages of the appearance of life?
- The balance between stability and radiation damage is a key issue for radiation therapy of cancer tumors, where the aim is to confine the irreparable damage to the tumor cells while sparing surrounding tissue.
- A single or double strand of DNA/RNA offers a nearly one-dimensional structure built up from a handful of specific units which can be studied in isolation and in well-defined sequences up to macromolecular size. A step-wise characterization of their dynamics may therefore be more feasible than for more monolithic biological systems (e.g. the large and three-dimensionally intricate structures of proteins).
- A DNA/RNA strand allows relatively long-range charge transport, which can be discussed in terms of electrons, holes, excitons or excimers/exciplexes[86, 87]. Combined with the information carrying capacity, this has led to discussions of applications in molecular machines and organic electronics[88, 89, 90].

The nucleobases (adenine, cytosine, guanine, and thymine/uracil) and nucleosides (nucleobase bound to sugar) all absorb strongly in the UV (mainly 230–280 nm, in the UVC band). For DNA macromolecules the absorption extends significantly into the UVB band ($\geq$280 nm) where more sunlight is available. The peak cross sections are approximatively $2 \times 10^{-18}\,\mathrm{cm}^2$ (molar extinction coefficients of $10^4\,\mathrm{M}^{-1}\mathrm{cm}^{-1}$) [87, 90]. UV-excitation leads to the lowest singlet state, denoted $S_{\pi\pi^*}$ (or equivalently $^1\pi\pi^*$), with an electron promoted from the highest occupied molecular orbital (HOMO) to the lowest normally unoccupied orbital (LUMO). The biologically relevant consequences of UV photoreactions in nucleic acids and the DNA macromolecule involves molecular dynamics on different size- and time-scales, and based mostly on the comprehensive reviews by Middleton *et al.* in 2009[87] and Barbatti *et al.* in 2015[90] a basic overview will be given in the following. Although studies of single nucleobases revealed sub-picosecond relaxation times already in year 2000[93, 94], it is only recently that theoretical

progress and experiments involving pairing and stacking into larger structures has begun to establish a more accurate picture of the biologically relevant photochemistry.

Considering first the case of separate molecules, experiments indicate rather similar rapid relaxations of the initial excitation, regardlessly of whether fluorescence or ion yield is studied as seen in Figure 12. The decay lifetimes of a few hundred femtoseconds are also relatively unaffected by whether the environment is vacuum, water, methanol or acetonitrile and by whether a sugar is attached to the base[87, 91, 95]. The explanation for the fast relaxation is that a conical intersection towards the ground state is reached

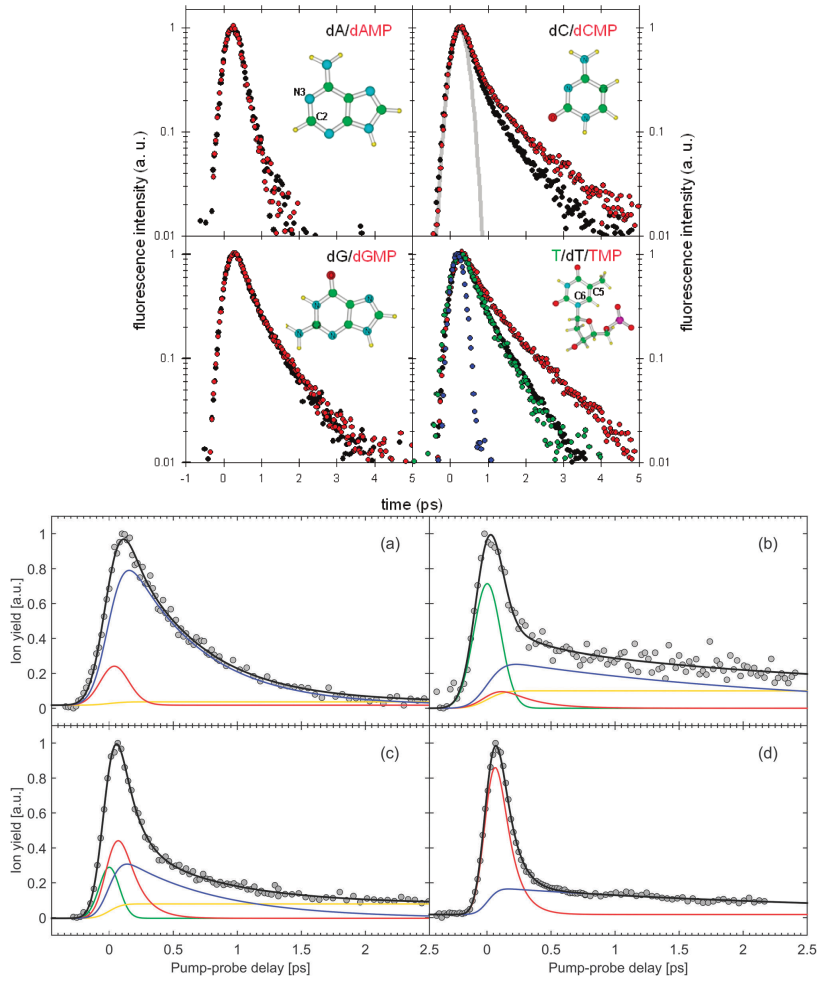

Fig. 12. – Ultrafast relaxation of excited states in nucleosides, from experiments using (top four) fluorescence after UV-photoexcitation (reprinted with permission from Ref.[91]) or (bottom four) ion yield after XUV-ionization and NIR-probing (reprinted with permission from Ref. [92]). In the top four panels nucleosides are shown in black, nucleotides in red, but among nucleobases only thymine (green) and uracil (blue) are included. The time resolution is indicated by an apparatus function (gray curve). The lower four panels show (a) adenosine, (b) guanosine, (c) cytidine and (d) thymidine. Note that the upper four and the lower four panels differ in the ordering of the bases by a swapping of the guanosine (b) and cytidine (c) panels.

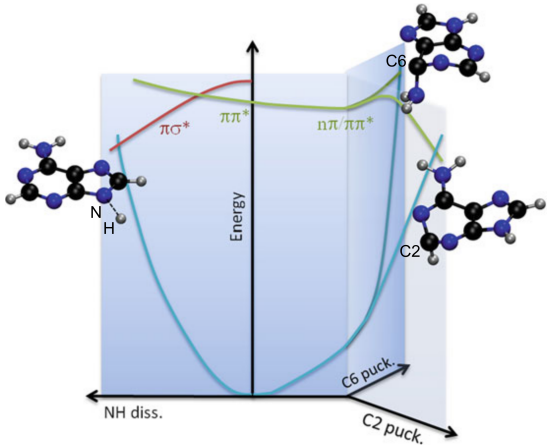

Fig. 13. – Schematic illustration of the main traits of potential energy surfaces near the Franck-Condon region for adenine (reprinted with permission from Ref. [90]). The UV-excited $S_{\pi\pi^*}$ is relatively flat but intersects the ground state which has steep gradients with respect to the three coordinates shown (one N–H dissociation and two puckering deformations of the carbon backbone).

with a large quantum yield and no significant potential energy barrier. The potential energy surface of the excited $S_{\pi\pi^*}$ state can be relatively flat with respect to the relevant vibrational coordinates while the main cause of the conical intersection is the increasing energy of the ground state when deviating from planar geometry. For adenine, Figure 13 illustrates the central potential energy landscape along two puckering (out-of-plane deformations) coordinates of the carbon backbone and one N–H bond elongation coordinate [90]. For uracil, it has been similarly demonstrated the presence of a conical intersection that is enabled by displacing a hydrogen atom from the molecular plane [91]. Gradually, the trajectory in the potential energy landscape converts electronic excitation energy into vibrational energy, and interaction with the solvent allows this to be dissipated as heat. Although the 4.1–5.4 eV range of energy deposited by the UV photon would be sufficient to break a bond, the efficient conical intersection and vibrational relaxation gives a high probability for the molecule to return to the ground state without any permanent change. The probability of reaching the favorable conical intersection may however be influenced by the presence of a $S_{n\pi}$ state[96, 97], not directly accessible by photoexcitation, but its role is not well understood – particularly in the pyrimidine bases (cytosine, thymine and uracil) the experimental findings have been hard to reconcile. It has also been noted that the $S_{n\pi}$ potential energy surface is very sensitive to the chemical environment[91, 90].

In the case of a strand of DNA or RNA, the adjacent nucleobases are stacked close enough to let the electron and hole be localized on adjacent nucleobases (a charge-transfer state) or delocalized over the pair of molecules[86, 87]. This is called an *excimer* (excited dimer) in the case of equal bases or an *exciplex* in the case of or two or more unequal bases. Particularly at the high-energy side of the UV-absorption band, excimer states may also be directly populated by the photoabsorption, but much uncertainty remains over the energetics of these states[98]. The probability for the initial excitation to be converted to an excimer is high according to experiments (in some cases above 50%)[86, 87], although simulations suggest that the rate is highly sensitive to the conformation of the bases

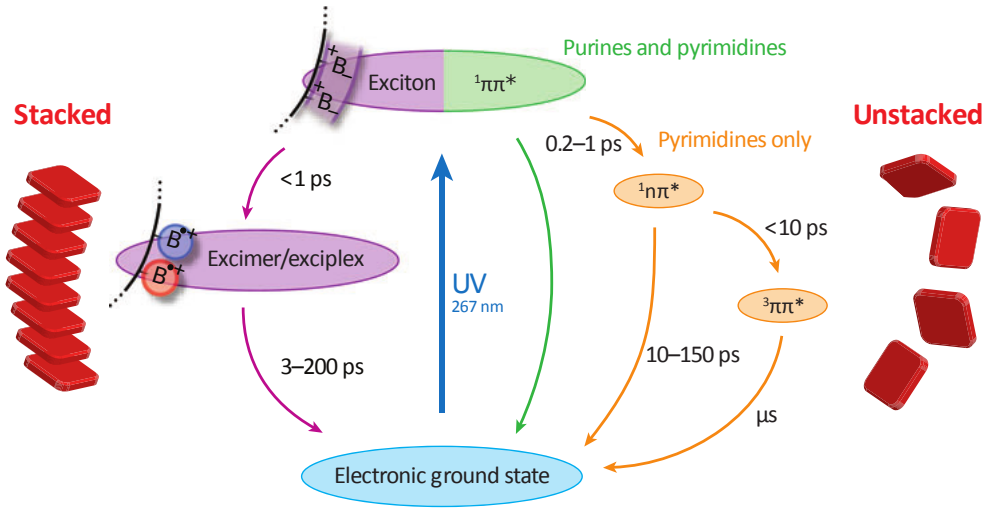

Fig. 14. – Illustration of ultrafast relaxation of nucleobases: the electron dynamics after UV-excitation to the singlet $\pi\pi^*$ state is strongly dependent on whether they are stacked in an RNA/DNA-strand or in the form of separate molecules. Reprinted with permission from Ref. [87].

(dependent on the flexibility of DNA, not occurring in the nominal geometry)[98]. The excimers have been shown to have comparably long lifetimes, from 10 to 200 ps [90, 98]. This means that the intrinsic photostability of isolated nucleotides due to fast relaxation to the ground state, does not trivially translate to stability of the DNA macromolecule. The main decay mechanism of the excimers seems to be recombination of the electron and hole on a single base, so that the local ultrafast intra-molecular reaction path can be followed to the ground state. Figure 14, taken from Middleton *et al.*[87], gives an overview of the time scales for the key relaxation paths now unravelled for stacked and free nucleosides.

The excimer formation in DNA/RNA strands is thus acting as a trap, extending the lifetime of the electronic excitation and delaying the dissipation into heat. While involving more than one nucleobase in the relaxation does open up more vibrational degrees of freedom[98], one may expect that a longer time of propagation on potential energy surfaces more than 3 eV above the ground state increases the risk of entering a reaction path towards structural damage. The most common type of genetic damage is cyclobutane-pyrimidine-dimer (CPD) formation, where two neighbouring pyrimidine bases (e.g. a -T-T- sequence) are fused, and this has been seen to occur within 1 ps[90]. Some studies showed additional dynamics (sub-picosecond proton transfer) between pairs of free complementary bases, but it does not seem to occur when the base-pairs are stacked into double-strand DNA[87]. The electronic excitation and the molecular dynamics thus appears fairly constrained to one of the strands in the double-helix[86]. This, and the fact that the excimer/exciplex lifetime is much longer than in isolated bases, might be rationalized as accepting a higher rate of DNA damage that is limited to a single strand, in order to minimize the risk of double-strand damage. In the presence of efficient repair mechanisms that can use the complementary DNA strand as template, the selective pressure for maintaining the genetic information would mainly be concerned with double-

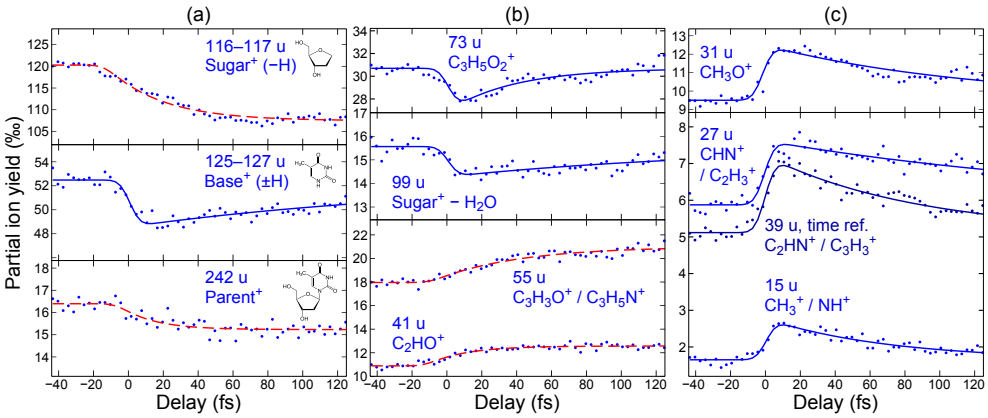

Fig. 15. – Pump–probe delay dependence of selected fragment ion yields from thymidine. The parent ion and the most abundant fragment ions are in panel (a), while (b) and (c) contain fragment ions with lower yield and lower mass. Reprinted with permission from Ref. [99].

sided disruptions. It is also plausible that selection of the nucleobases occurred during the prebiotic stage before genetic information needed to be preserved, simply by virtue of their remarkably high UV-stability as individual molecules[91].

In addition to the UV photoexcitation described above, tissue and DNA can be exposed to high-energy ionizing radiation from cosmic rays, radioactive materials and during radiation therapy of cancer tumors. As water is the most abundant molecule in the human tissue, actual DNA damage is mainly occurring via secondary electrons or radical molecules. The secondary electrons have a continuous distribution of low kinetic energies, below roughly 30 eV, just like the XUV attosecond pulses most easily produced from a visible or NIR laser. We have therefore used attosecond pulses as a proxy for depositing this amount of energy in nucleobases and nucleosides, to start exploring all the ultrafast relaxation pathways resulting from the strong non-adiabatic couplings in a higher energy range than the UV, and typically after ionization of the molecule.

One study was made to compare thymine with its (deoxyribo-)nucleoside thymidine [99], the results of this investigation are shown in Figure 15. As in the previous Section (Figure 8), a 4.5 fs NIR laser pulse is used as probe and mass spectra of the ionic fragment are recorded as function of the probe delay.

The stability of ionized thymidine is relatively low, with the intact parent ion representing only 1.6 % of the total ion yield, while the ionized sugar-side of the molecule accounts for 12 % and the ionized base-side 5 % Absorption of the NIR probe after the XUV further facilitates fragmentation of the cation, increasing the yields of small ionic fragments and reducing the yield for large fragments, but this effect decays in most cases if the NIR pulse is sent much later – indicating timescales for the relaxation of the thymine ion away from the states and geometries where the probe can influence the reaction path. Lifetimes from 40 to 210 fs were fitted for these decays, and with more than 68 % confidence the lifetime relating to $C_3H_5O_2^+$ (part of the sugar) production is shorter than those relating to $(\text{base})^+$ and the ejection of CHN^+ or $C_2H_3^+$.

For some fragments ($(\text{sugar})^+$ and C_2HO^+) the effect of the probe grows stronger rather than weaker for later probing times, meaning that a reaction path needs to be followed (represented by transient lifetimes of 20–50 fs) before they become susceptible to

the probe's effect. The probe is enhancing the C_2HO^+ yield and depleting the sugar$^+$, so if C_2HO^+ is assigned as coming from the sugar-side of the molecule the probe-controlled branching between these final-state ions occurs after the charge has been confined to the sugar side. However, from the mass spectrum it is not certain that 41 u is only C_2HO^+, the same mass could have a contribution from $C_2H_3N^+$ which would be from the base side.

In the absence of the sugar part, the base, thymine, accounts for 7 % of its mass spectrum, which is rather similar to its 5 % yield as fragment from thymidine where the base ion was the most abundant fragment. Considering also that thymine gives fewer fragment ions without any dependence on probe delay[99], it seems likely that the most vivid, or most easily probe-influenced, hole dynamics in thymidine was occurring on the sugar side. The observed timescales of transient states are consistent with nuclear motion on potential energy surfaces, towards internal conversion to other electronic states. The potential energy surface region explored before probing does not appear to excite any fast vibrational modes, since as all the dynamics could be fitted by single-exponential curves without oscillations. Although oscillations with periods below the 3 fs step size can not be excluded, it can be mentioned that no convincing hints of faster dynamics were seen in this specific case. As mentioned above, a broadband XUV pulse populates a superposition of many valence-hole states, which tend to be less localized, making it far from expected that the total charge density would exhibit clear oscillations at any particular site. Decoherence due to rapid nuclear motion would further reduce the chance of a sustained beating.

6. – Techniques for the production of biomolecules in gas-phase

Experiments on the spectroscopy and dynamics of biomolecules in the gas phase are in the minority when compared to studies in solution. However, when using extreme ultraviolet (EUV) attosecond light pulses to interrogate biomolecular dynamics, studies are generally only possible for isolated molecules in vacuum. As extreme ultaviolet light (¡ 100 eV) has a penetration depth of only 100 nm in water, which is smaller than liquid jet diameters, the application of transient absorption spectroscopy to the attosecond regime is challenging. As progress is made towards producing attosecond pulses at in the water window (280-540 eV) and beyond, via either harmonic generation or free electron lasers, greater water penetration will be possible [100, 101, 102, 103]. This will open up attosecond transient absorption spectroscopy of inner shell transitions for biomolecules in solution. A template for such measurements has already been demonstrated in the gas phase where K-shell absorption spectroscopy with a free electron pulse has been employed to interrogate ultrafast internal conversion in the DNA base thymine. Other atomic and molecular targets have been similarly probed [104], but so far no equivalent measurements have been made for biomolecules in solution.

An alternative approach for attosecond studies of biomolecules in their native environment is to use electron at the surface of a liquid jets containing solvated biomolecules. Recently a number of experiments have been set up to acquire photoelectron spectra from liquid jets, with the ultrafast behaviour of solvated electrons of particular interest [105, 106, 107]. Again these techniques have yet to be applied to solvated biomolecules and in such experiments the background signal from the solvent could be overwhelming. A more achievable solution in the new future could come from studying partially solvated single molecules in a size selected cluster [108, 109].

While gas phase measurements are not an exact analog of in vivo biomolecular func-

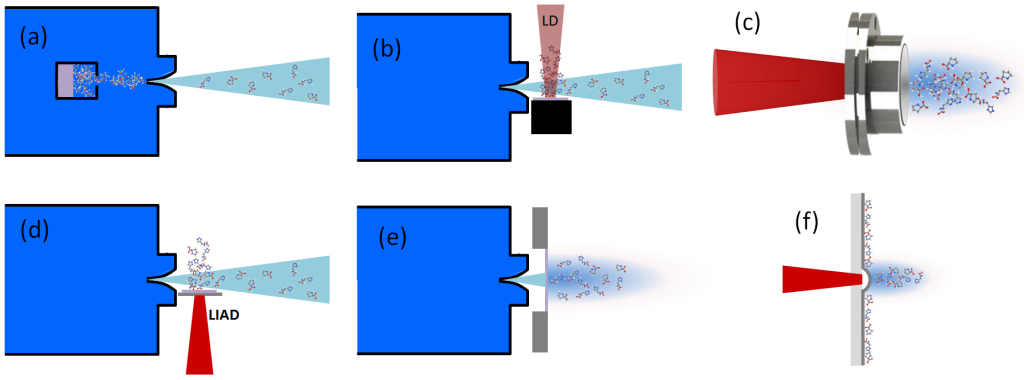

Fig. 16. – Different schemes for producing gas phase targets of cooled labile molecules by entraining them in a gas jet produced by a pulsed valve; (a) A miniature filled cartridge within the valve is heated to volatilise the sample; (b) Laser desorption (LD) of sample from an absorbing substrate such as graphite; (c) Laser induced acoustic desorption(LIAD) from a thin metal foil; (d) LIAD coupled to a pulsed valve; (e) Pulsed valve induced desorption; (f) Blister based laser induced forward transfer (BB-LIFT) from a metal film on a glass substrate

tion, the ability to study the intrinsic properties of key biomolecular sub-units via experiment and theory is necessary for gaining fundamental insight into biological processes. For some biological chromophores which are embedded in proteins, their environments are actually closer to vacuum than solution. For example mammalian vision is initiated by an ultrafast isomerisation of the retinal chromophore inside the rhodopsin protein[citeGaravelli1997,Gai1998 and the absorption spectrum of the green fluorescent protein chromophore in vacuum is closer to that found in the protein than in solution [110]. Therefore the study of ultrafast processes in biomolecules in the gas phase is relevant, particularly those approaching the attosecond regime. The initial response of biomolecular systems to instantaneous ionization events (driven by high energy photon or particle impact) has until recently been out of reach to experimentalists. With the advent of attosecond technology, such processes are now ripe for study but require pure, dense, and stable targets of gas phase biomolecules.

The development of electrospray ionization (ESI) and matrix-assisted laser desorption and ionization (MALDI), for which the Nobel Prize for Chemistry was shared in 2002 [111, 112], has dramatically stimulated studies of biomolecules in the gas phase. These techniques were particularly useful for analytical and structural studies as the molecules tended to be protonated or de-protonated allowing direct coupling to mass analyzers without any additional ionization source. ESI is a particularly soft process which is capable of introducing very large molecules such as proteins into a vacuum. This is achieved by applying a strong electric field at the tip of a capillary containing a solution of the biomolecule. A spray of highly charged droplets is produced with the solvent gradually being evaporated from the droplet due to Coulomb explosion so that only charged, isolated ions remain. Molecular densities produced from ESI are generally too low to be useful for most dynamical studies of biomolecules, although some researchers have overcome these challenges with innovative experiments [113, 114, 115, 116].

A number of alternative techniques have been exploited in order to create gas-phase targets of neutral biomolecules. For smaller building blocks such as nucleobases and

amino acids, direct vaporization from an oven has been effectively used for many years, albeit production of intact molecules is not guaranteed. In order to limit the time for which the molecules experience elevated temperatures and hence avoid de-composition, various schemes shown in Figure 16 are employed.

Expansion of a high-pressure rare gas into vacuum produces a cold jet into which sample molecules can be entrained and cooled via collisions[117]. This is shown in Figure 16(a) where molecules are volatilised by heating a sample contained within the valve. This works effectively for most molecules but pick-up of larger molecules is more difficult and as they are harder to evaporate and have more internal energy which is cooled at a slower rate. In these situations a heavy gas such as xenon is needed. This scheme uses the sample more efficiently than if the oven is outside the valve where a lower fraction of molecules are dragged into the stream. However, the advantage of the latter is that production of clusters is suppressed which is preferable for studies of isolated molecules.

For molecules which have very low vapour pressures, alternative techniques are required. These are based on pulsed laser desorption (LD) from a substrate on which the sample has been deposited. This can result in a very rapid heating rate, up to 10^{12} K/s, which causes ablation of the substrate due to a temperature increase of several thousand kelvin from which the sample is also liberated into vacuum. With judicious choice of substrate and wavelength, direct heating of the sample is avoided allowing heavy biomolecular species to be produced[118]. Graphite is a popular substrate choice, which can also be mixed and compacted with the sample[119, 120], but silicon[121] and nano-patterned[122] surfaces have also been used. In MALDI, a matrix which absorbs strongly at the laser wavelength also acts to ionize the sample via charge transfer, allowing direct coupling to a mass spectrometer. As MALDI ionization efficiency is relatively low ($< 10^{-4}$)[123], it also produces a dense plume of neutral molecules as well as ions[124], but the complex mix of molecular components makes it less suitable for studies of requiring single component gas phase targets.

The high temperatures generated by LD might seem incompatible with desorption of intact molecules, especially when the activation energies for molecular decomposition are lower than the desorption energy. However, as these temperatures are short-lived and the mobility of sample molecules on the substrate is restricted, fewer reaction coordinates for dissociation are accessible than for desorption. So the desorption rate is much higher than the dissociation rate as it is entropically more favourable[125, 126].

Although LD can produce very large intact molecules they need to be cooled soon after they are desorbed. This is typically achieved by positioning the substrate and sample as close as possible to the nozzle of a pulsed valve without disrupting the gas flow as shown in Figure 16(b). The high number of molecules liberated from the substrate every pulse compensates for the low efficiency of entraining the molecules into the gas stream and transporting to the interaction region. Therefore, LD has been successfully exploited by a number of groups for spectroscopy of biomolecules[127, 128, 129, 130, 131, 132]. The high sample depletion rate can be mitigated by translation of the substrate target area to bring new sample into focus which is essential for modern experiments conducted at high repetition rates[133].

When a high sample purity is required, LD might not be suitable due to presence of substrate contaminants in the gas jet. A cleaner alternative is laser induced acoustic desorption (LIAD) which also has the advantage that the sample is never directly irradiated by the desorption laser. The basic scheme is shown in Figure 16(c) where the sample is deposited on a thin foil but the laser is focussed onto the reverse side of the foil. This technique has been around for more than years[134] but it is only

in recent years that it has come into its own. Unlike MALDI where the desorption is immediately evident from mass spectrometry of the ions produced, probing the neutral plumes requires the use of single-photon ionization[135, 136], electron impact[137], chemical ionization[138, 139, 140], or with the advent of table-top femtosecond lasers, strong field ionization[141, 142, 143].

The foil is typically around 10–15 µm in thickness and made of tantalum or titanium. Sample can be deposited on the surface by drying out droplets or directly rubbing onto the surface. However, with these techniques it is difficult to get uniform coverage and as a result the shot-to-shot variation can be very large. Sample depletion is also an issue. Therefore, fine aerosol deposition and mechanisms to translate fresh samples into the desorbing lasers path are much more effective for experiments requiring better target stability[143]. This technique has produced plume densities which have been estimated at a lower limit of $10^9\,\mathrm{cm}^{-3}$ [141, 143]. This is lower than those achievable by direct LD but produces much cleaner and cluster free plumes. In addition, although the molecules are liberated with internal temperatures greater than typically 150 °C, soft ionization techniques have demonstrated that small biomolecular species such as amino acids and DNA nucleosides can be desorbed without any fragmentation[92, 144].

The exact mechanism is still not fully understood but LIAD is somewhat of a misnomer since it is clear that any acoustic waves set up in the foil do not contribute to the desorption process. It has been found that there is a significant delay of about 10 microseconds between application of nanosecond laser pulses and liberation of molecules from the surface which is orders of magnitude longer than the duration of any acoustic waves in the foil[135, 141, 143]. Molecules are also ejected with a central velocity which is independent of the power of the desorbing laser suggesting that the mechanism is related to the mechanical properties of the sample deposited on the foil[135, 143, 145]. The mis-match between the properties of the surface and sample sitting on it is believed to be responsible for stress-induced fracturing of sample islands resulting in release of isolated molecules into the vacuum. This could be caused by the transient thermal stresses induced by the laser, but it has also been shown that as good, if not better, outcomes can be obtained from steady state heating with a CW laser[71, 146]. So a better name for the technique might be Laser Induced Thermal Desorption (LITD).

While LIAD or LITD is a softer desorption technique than LD and has been used for experiments without additional cooling, the high internal temperatures mean this is generally not possible for more labile biomolecules. Therefore, there is interest in developing a similar scheme as that for LD where the molecules are entrained into a gas jet as shown in Figure 16(d). This would produce a pure, cold molecular target, but is unlikely to produce the target densities achievable with direct LD.

More recent developments have also focussed on indirect coupling of mechanical energy to a thin foil to liberate samples. For instance a pulsed valve placed directly behind the foil has been used to generate ions of proteins which had been deposited on the foil along with an ionising matrix as shown in Figure 16(e). This was achieved at ambient pressure with the molecular ions produced directed towards the inlet of a mass spectrometer[147].

Lasers have also been used to generate similar forward momentum to nanoparticles attached to a thin metal film by a technique known as Laser Induced Forward Transfer (LIFT). Initial developments used a thin metal coating deposited on a glass substrate which is heated and vaporized to eject the sample molecules[148]. However, recently a thicker film has been used so that vaporisation is avoided but formation of a blister transfers momentum to the sample liberating it into the gas phase without substantial

TABLE I. – *Comparison of the advantages and disadvantages of different techniques for generating biomolecules in the gas phase. ESI: Electrospray Ionization, MALDI: Matrix Assisted Laser Desorption and Ionization, LD: Laser Desorption, LIAD: Laser Induced Acoustic Desorption, LITD: Laser Induced Thermal Desorption, BB-LIFT: Blister Based Laser Induced Forward Transfer.*

Technique	**Advantages**	**Disadvantages**
Oven	simple, can be incorporated into pulsed valve, consistent density	unsuitable for low vapour pressure samples, thermal decomposition for labile molecules
ESI	gentle process capable of producing macromolecules, ions produced which can be directly coupled to a mass analyzer	very low densities, no neutral species
MALDI	large numbers of molecules liberated per laser shot, ions produced which can be directly coupled to a mass analyzer	poor shot-to-shot stability, quick sample depletion, plume contains matrix
LD	large numbers of molecules liberated per laser shot, intact species produced if immediate entrained in gas jet	poor shot-to-shot stability, quick sample depletion, plume contains substrate
LIAD/ LITD	moderate density, clean, intact, neutral targets produced, molecules not directly irradiated, no clustering	relatively high internal temperatures but has potential to be mitigated with gas jet cooling schemes, quick sample depletion
BB-LIFT	Effective for producing large nanoparticles or biomolecules, clean plumes	Yet to be demonstrate as an effective and stable biomolecule gas phase target

heating. This Blister Based Laser Induced Forward Transfer (BB-LIFT)[149, 150] scheme is shown schematically in Figure 16(f). The blister formation has been found to be more effective with a femtosecond rather than a nanosecond desorption laser, as it offers more efficient mechanical coupling to the film rather than heating. Liberation of large nano- or bio-particles is possible as the momentum transfer in these techniques increases with the mass of the molecule.

So a range of established and new techniques are available to study biomolecules in the gas phase. The relative merits of these techniques are summarised in Table I, If the unique capabilities of new facilities delivering attosecond and free electron laser pulses are to be fully exploited in the future, means that gas phase targets are needed which consistently produce a high density and purity of the neutral, low temperature biomolecules. Such sources are beyond current capability but with augmentation of existing techniques such as LIAD/LITD with pulse gas jet cooling and investigation of new techniques such as BB-LIFT, then this will be open up a variety of studies of ultrafast biomolecular dynamics.

7. – Theoretical models

A theoretical description of laser-matter interactions using attosecond light sources requires of a time-dependent treatment. This has to describe preparation of the initial wave packet by the pump pulse, the subsequent evolution of the non-stationary electronic-nuclear state, and the result of the final probing. After the initial pulse, the ionized electron departs very quickly, leaving behind a coherent superposition of cationic states described by a density matrix. Also nuclear motion can be considered frozen in the

first few femtoseconds, although in many situations the strong out-of-equilibrium state will trigger a fast nuclear dynamics. Finally description of the final probing generally employed in the experiments, which is detection of the ions produced by the NIR probe pulse, is particularly difficult. We shall describe the tools and approximations employed in our recent studies, with reference to other work in the literature.

Recent applications to molecules of biological relevance have made use of two different approaches, both based on the density functional theory (DFT) formalism.

(i) the static-exchange DFT (SE-DFT) method plus time-dependent perturbation theory has been employed for the preparation of the initial wave packet, which has been then freely propagated in the basis of Slater determinant built from Kohn-Sham orbitals. Accurate wavepacket propagation is a strong point of the present approach, which distinguishes from many previous studies of charge migration, where an ad hoc hole creation in a frozen orbital (Sudden Approximation, SA) has been employed [151, 3, 5]. The SE-DFT method [152, 153, 154, 155] has been amply validated in photoionization studies, obtaining good quality ionization cross sections and angular distributions, from simple systems like N_2 or CO [156] to biochemically relevant molecules such as the amino acid phenylalanine [71]. It provided the first reliable description of the electronic wave packet created in the ionization of a biomolecule by a broadband attosecond pulse [71, 146]. Previous applications of this method have either ignored the nuclear motion (fixed-nuclei approximation, FNA) or have included at most a single nuclear degree of freedom, which is appropriate for diatomic molecules [156, 157] or for small polyatomic molecules in problems where a single vibrational mode is active [158, 159].

(ii) As a further step both electronic and nuclear dynamics following initial preparation have been addressed also employing full time dependent DFT (TDDFT) coupled with nuclear motion described by Ehrenfest Dynamics, the TDDFT-ED method, as implemented in the CPMD package [160]. Several Ehrenfest dynamics studies have been also performed in the literature with ab-initio approaches, starting from the SA or ad-hoc coherent superpositions of states [161, 69].

(iii) Finally from the evolution of the wave packet the time dependent electronic density is computed, and it is assumed that its oscillations around selected chemical groups (the amino groups in amino acids) is strongly connected with the experimental probe. This assumption is a posteriori validated by the good agreement with experimental observations [71] and further validated by a new theoretical analysis [162].

In this section, we will first summarize the essence of the SE-DFT method for the wave packet preparation and then briefly describe the basic equations employed to describe the evolution of the N and $N-1$ electron densities associated, respectively, with the neutral and the cationic system. Finally, we will explain the implementation of the TDDFT-ED method to account for the nuclear motion during the evolution of the electronic wave packet created in the ionization step.

7˙1. *The initial electronic wavepacket .* – Attosecond pulses are typically of low intensity with frequencies in the XUV spectral domain, and their interaction with matter is accurately described by first-order time-dependent perturbation theory. Thus, the wave packet created upon the interaction of the molecule with such pulses can be written in the basis of molecular eigenstates as

$$\Psi(\vec{r}_1,...,\vec{r}_N,t) = c_0(T)\ \mathrm{e}^{-iE_0t}\ \Psi_0(\vec{r}_1,...,\vec{r}_N) + \\ + \sum_{\alpha,l}\int c_{\alpha,l}(\varepsilon,T)\mathrm{e}^{-i(E_\alpha+\epsilon)t}\ \Psi^l_\alpha(\vec{r}_1,...,\vec{r}_N,\varepsilon)\ d\varepsilon \tag{2}$$

where $\Psi_0(\vec{r}_1, ..., \vec{r}_N)$ is the ground state of the neutral molecule and $\Psi^l_\alpha(\vec{r}_1, ..., \vec{r}_N, \varepsilon)$ describes the N-electron system where one electron is in the continuum with energy ϵ and angular momentum l, and the ion is left behind with a hole in the α orbital. The time evolution of the wave packet is given by the stationary phases in the absence of the field ($t > T$, where T is the pulse duration) and the corresponding amplitudes at the end of the pulse:

$$c_0(T) \approx 1$$
$$c_{\alpha,l}(\varepsilon, T) = -i \, \langle \Psi^{\varepsilon,l}_\alpha | \hat{\mu} | \, \Psi_0 \rangle \int_{-\infty}^{\infty} \vec{\mathcal{E}}(t) \, \mathrm{e}^{i(E_\alpha + \varepsilon - E_0)t} dt, \tag{3}$$

where $\langle \Psi^{\varepsilon,l}_\alpha \mid \hat{\mu} \mid \Psi_0 \rangle$ is the dipole transition matrix element connecting the ground and a continuum state, $\hat{\mu}$ stands for the dipole operator (here we have used the length gauge form of this operator), the time integral is the Fourier transform of the electric field, $\vec{\mathcal{E}}(t)$, and $(E_\alpha + \varepsilon - E_0)$ is the energy absorbed by the system. The field is defined from 0 to T using experimental temporal envelopes, $F(t)$, in the form $\vec{\mathcal{E}}(t) = F(t) \sin(\omega t + \phi)\vec{\epsilon}$, with $\vec{\epsilon}$ being the polarization vector and ϕ the carrier-envelope phase, which is fixed to zero. Due to the definition of the field, the integral in equation (3) reduces to the interval $[0, T]$.

The final continuum states and transition dipole moments are obtained by using the SE-DFT method as described in [153, 154, 155], generally employing the LB94 functional. Starting from the ground state density of the neutral molecule, bound and continuum eigenvectors of the Kohn-Sham hamiltonian are obtained in a multicentric (LCAO) B-spline basis which is particularly suitable to represent the continuum functions at any desired distance from the molecular center of mass. Accurate multichannel solutions associated with a particular electron energy are obtained by using the Garlekin approach [163, 164]. Ionization energies are estimated from the DFT eigenvalues, after shifting to the value of the first ionization potential computed using the outer-valence Green′s function method. We refer to the literature for details of the approach and actual calculations.

7˙2. *N-electron and $(N-1)$-electron densities.* – A practical way to visualise charge migration in large molecules is to compute the electron density in the remaining ion, assuming that the dynamics of the photoelectron and that of the cation can be decoupled. This approximation will be valid as long as the interaction of the leaving photoelectron and the ion is negligible, for instance, if the electron is rapidly ejected. To validate this approximation within the SE-DFT formalism described above, we will compare the electron densities of the N and $(N-1)$-electron systems. In the first case, the effect of the continuum electron is explicitly included. In the second case, a common procedure is to make use of the reduced density matrix formalism to get rid of the ejected electron.

We compute the time-dependent one-particle electron density from the perturbed part of the N-electron wave function, as

$$\rho_N(\vec{r}_1, t) = N \int d\vec{r}_2 \ldots \int d\vec{r}_N \, \left| \Psi_N(\vec{r}_1, ..., \vec{r}_N, t) \right|^2 \tag{4}$$

where $\Psi_N(\vec{r}_1, ..., \vec{r}_N, t)$ is the N-electron wave packet created by the XUV pulse, which

can be written, as in Eq. (2), as an expansion over N-electron continuum eigenstates:

$$\Psi_N(\vec{r}_1,...,\vec{r}_N,t) = \mathcal{N}\sum_{\alpha,l}\int d\varepsilon\; c_{\alpha,l}(\varepsilon,T)\Psi^l_\alpha(\vec{r}_1,...,\vec{r}_N,\varepsilon) \tag{5}$$

with $\mathcal{N}$ being a normalization factor. The corresponding expression for the one-particle density in the basis of spin-orbitals can be written as

$$\begin{aligned}\rho_N(\vec{r}_1,t) = \sum_{\alpha,l}\int \mathrm{d}\varepsilon \Bigg[\Big(\sum_{\alpha'\neq\alpha} |\varphi_{\alpha'}(\vec{r}_1)|^2 + |\varphi_l(\vec{r}_1,\varepsilon)|^2 \Big)\; |c^l_\alpha(\varepsilon)|^2 \\ - \sum_{\alpha'\neq\alpha} c^{l\,*}_\alpha(\varepsilon)\; c^l_{\alpha'}(\varepsilon)\; \varphi_\alpha(\vec{r}_1)\; \varphi_{\alpha'}(\vec{r}_1)\; \mathrm{e}^{-i(E_{\alpha'}-E_\alpha)t} \\ + \sum_{l'}\int \mathrm{d}\varepsilon'\; c^{l\,*}_\alpha(\varepsilon)\; c^{l'}_\alpha(\varepsilon')\; \varphi_l(\vec{r}_1,\varepsilon)\; \varphi_{l'}(\vec{r}_1,\varepsilon')\; e^{-i(\varepsilon'-\varepsilon)t} \Bigg],\end{aligned} \tag{6}$$

where $\varphi_\alpha(\vec{r}_1)$ is a Kohn-Sham spin-orbital and $\varphi_l(\vec{r}_1,\varepsilon)$ is a continuum spin orbital. The above expression has a stationary part, the first term, and two other terms that lead to variations of the electron density with time. The periodicity of the oscillations in the density are dictated by the energy differences between cationic states (second term) and between continuum orbitals themselves (third term). The former are due to the fact that electrons can be ejected with the same energy and angular momentum from different orbitals. The third term effectively vanish in the neighborhood of the molecule if one waits long enough until the ejected electron is far away from the molecule [70]. When this limit is reached, one can then ignore the photoelectron and define a one-particle electron density from an $(N-1)$-electron system. For this purpose, we rely on the reduced density matrix formalism, where the N-electron wave function is first projected into the continuum wave functions and then integrated over all continuum energies, thus leading to an $N-1$ ionic electron density

$$\begin{aligned}&\rho^{ion}_{N-1}(\vec{r_1},\vec{r}_2,...,\vec{r}_{N-1},t) = \\ &\sum_l \int d\varepsilon\; \langle \varphi_l(\vec{r}_N,\varepsilon)\; e^{i\varepsilon t}|\Psi_N\rangle_{\vec{r}_N}\langle\Psi_N|\varphi_l(\vec{r}_N,\varepsilon)\; e^{-i\varepsilon t}\rangle_{\vec{r}_N},\end{aligned} \tag{7}$$

in which the brackets indicate an integral over the N-th spatial coordinate. We define the one-particle electron density of the ion as

$$\rho^{ion}(\vec{r},t) = \int \rho^{ion}_{N-1}(\vec{r},\vec{r}_2,...,\vec{r}_{N-1},t)\, d\vec{r}_2,...,d\vec{r}_{N-1} \tag{8}$$

where one has now an integral over the spatial coordinates of $N-2$ electrons instead of $N-1$ electrons. Substituting (5) in the above equation gives the following expression for the electron density of the ion:

$$\rho_{ion}(\vec{r},t) = \sum_\alpha \left[\sum_{\alpha'\neq\alpha} \gamma^{(ion)}_{\alpha'\alpha'} \right] \varphi^2_\alpha(\vec{r})$$

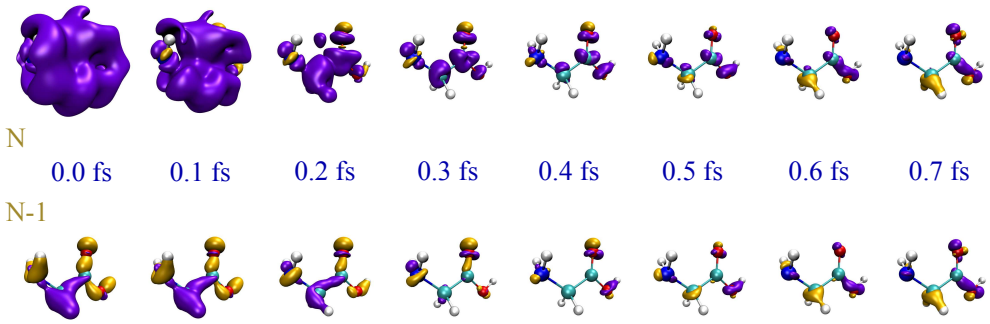

Fig. 17. – Comparison of hole densities corresponding to N and $N-1$ electron systems right after the action of a sub-300-as XUV pulse. For the sake of clarity, the hole density has been referred to its time-averaged value, so that yellow and purple colors indicate, respectively, excess and default of charge with respect to the average hole density. Upper rows: N-electron system (see text). Lower rows: $(N-1)$-electron system. Iso-surfaces with values $8{\times}10^{-4}$ and $-8{\times}10^{-4}$ a.u. are plotted in yellow and purple, respectively. Zero time is taken right at the end of the XUV pulse.

$$- \sum_{\alpha} \sum_{\alpha \neq \alpha'} \gamma^{(ion)}_{\alpha\alpha'} e^{-i(E_\alpha - E_{\alpha'})t} \varphi_\alpha(\vec{r}) \varphi_{\alpha'}(\vec{r}), \tag{9}$$

where we have used the reduced density matrix, $\gamma^{(ion)}_{\alpha\alpha'}$ defined as

$$\gamma^{(ion)}_{\alpha\alpha'} = \sum_{l} \int d\varepsilon \; c_{\alpha\varepsilon l}(T) c^*_{\alpha'\varepsilon l}(T). \tag{10}$$

For illustrative purposes, it is common to define the hole density as the difference between the electron density that corresponds to the initial state of the neutral target and that of the cation, $\rho_{hole}(\vec{r},t) = \rho_{neutral}(\vec{r}) - \rho_{ion}(\vec{r},t)$. For consistency, in the case of the N-electron system we will use a similar expression, where $\rho_{ion}(\vec{r},t)$ is now replaced by $\rho_N(\vec{r},t)$ given in equation (6). The electron density of the neutral molecule is simply given by the sum of the squares of the occupied Kohn-Sham orbitals, $\rho_{neutral}(\vec{r}) = \sum_\alpha \varphi^2_\alpha(\vec{r})$, and thus the hole density is simply given by

$$\begin{aligned} \rho_{hole}(\vec{r},t) = & \sum_{\alpha} \left[1 - \sum_{\alpha' \neq \alpha} \gamma^{(ion)}_{\alpha'\alpha'} \right] \varphi^2_\alpha(\vec{r}) \\ & + \sum_{\alpha} \sum_{\alpha \neq \alpha'} \gamma^{(ion)}_{\alpha\alpha'} e^{-i(E_\alpha - E_{\alpha'})t} \varphi_\alpha(\vec{r}) \varphi_{\alpha'}(\vec{r}). \end{aligned} \tag{11}$$

To illustrate the effect of the photoelectron on the evolution of the electron density in the remaining cation, we have chosen the most stable conformer of the glycine molecule. We have ionized this molecule by using the experimentally available sub-300-as pulse reported in [71], which has a spectral energy bandwidth covering photon energies from 18 to 35 eV. The chosen glycine conformer is the most abundant one at room temperature ($\simeq 60\%$ [165]). For simplicity, we have assumed that the positions of the nuclei remain

frozen during the time evolution. Figure 17 shows the early evolution of the hole density, $\rho_{hole}(\vec{r}, t)$, obtained by including (top row) and excluding (bottom row) the ionized electron. As can be seen, the ejected electron spreads around the entire molecule when $t < 0.2$ fs, so that one cannot ignore its presence in the evaluation of the hole density. Later on, the ionized electron disappears from the vicinity of the molecular skeleton, but the correlation effects induced on the dynamics of the remaining cation are still visible, up to $t \sim 0.7$ fs. At longer times, the evolution of the hole density is practically the same as that resulting from ignoring the ionized electron.

7˙3. *Classical Ehrenfest nuclear dynamics.* – The electron density calculated just after the interaction with the attosecond pulse can be used as the starting point for TDDFT-ED calculations that describe the evolution of the $(N-1)$-electron density by taking into account the nuclear motion and its coupling with the electron dynamics. To do so, existing TDDFT methods must be extended to allow for an initial electronic density associated with a coherent superposition of one-hole states instead of a single electronic state. Thus one must first project the Kohn-Sham (KS) orbitals obtained from the static exchange DFT calculations (defining the density in eq 9) into the KS orbitals that initialize the time-dependent Kohn-Sham propagation in order to consistently define a new reduced density matrix γ_{ij}. In recent studies, this has been done in the framework of the KS DFT methodology as implemented in the CPMD package [160], in which nuclear dynamics is treated within the Ehrenfest formalism. The calculations were performed by using a plane wave basis and a large tetragonal box containing a single molecule. Following the standard procedures, core electrons were replaced by pseudo-potentials of the normal Troullier-Martins form [166]. Energies and forces were evaluated using the Kleinman-Bylander scheme [167] and the exchange-correlation potential was represented by using the generalized gradient approximation PBE functional, which is computationally more convenient than the LB94 one used in the static exchange DFT calculations when a basis of plane waves is used. The numerical integration that solves the equations of motion with the CPMD code was performed by using an iterative procedure based on a two-step Runge-Kutta propagator [168], which ensures an accuracy of the order of $\delta(t^3)$.

This methodology has been used to investigate coupled electron-nuclear dynamics in the most stable conformer of glycine [79] induced by the attosecond pulse reported in [71]. For computational convenience, instead of monitoring the electron density itself, we will track the evolution of the spin density after the interaction with the attosecond pulse, $\rho_s(t') = \rho_{up}(t') - \rho_{down}(t')$, i.e. the difference between the *up* and *down* spin densities. For a better visualization, we will refer the spin density at a given time t to the initial spin density at time zero, $\rho_d(t') = \rho_s(t') - \rho_s(t' = 0)$. This relative spin density thus provides information about the time evolution of the unpaired electron [169, 69] with respect to the initial density, as defined in eq. 9. Fig. 18 shows snapshots of $\rho_d(t)$, spanning a 16-fs time-lapse, obtained by including and excluding nuclear motion.

In earlier works [1, 170, 70, 171], in which the electron is removed from a well-defined, usually localized molecular orbital, pronounced charge oscillations between different atomic sites have been observed, mainly as a consequence of the spatial localization of the initial hole state, which eventually migrates through the molecular backbone. The results presented in Fig. 18 show that, with an attosecond pulse, the situation is completely different, since the pulse generates a coherent superposition of many one-hole states and, consequently, the oscillations are partly smeared out both in time and space. However, as can be seen in Fig. 18, significant charge fluctuations around the different

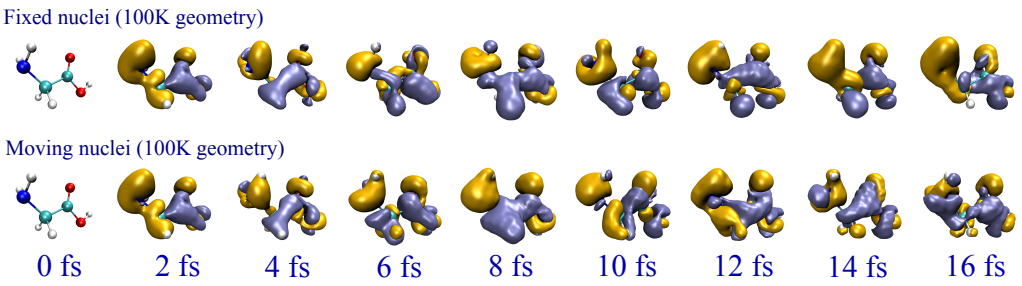

Fig. 18. – Spin density at different times after interaction of the XUV attosecond pulse with the glycine molecule. The spin densities at $t > 0$ are referred to the corresponding spin densities at $t = 0$ evaluated at the end of the pulse. Notice that, as a consequence of this choice, no spin density can be seen at $t = 0$. The XUV electric field is oriented along the N-C_β axis in all cases. The two rows show the spin densities obtained by starting from the equilibrium (100 K) geometry, for clamped and moving nuclei, respectively.Iso-surfaces with values $+/-0.001$ a.u. are colored in blue/yellow.

atomic centers are still visible, in agreement with previous theoretical and experimental work on the phenylalanine amino acid [71]. The calculated densities obtained for fixed and moving nuclei look very similar during the first 8 fs, thus indicating that nuclear rearrangements and non adiabatic effects play a minor role during the early stages of the wave packet evolution. Differences begin to be apparent and become progressively more pronounced at later times. The time interval during which nuclear dynamics is irrelevant is similar to that found in previous works on glycine [70] and other molecules [172, 173] where the ionization step was neglected.

7˙4. *Other theoretical approaches.* – Addressing the various steps outlined in a single coherent approach is extraordinarily difficult, although vigorous development is pursued in the separate areas. Initial state preparation by the pump pulse appears rather well established in the perturbative regime, and several approaches for molecular cross section calculation are available (see [9] and references therein), although the complexity of biological molecules can limit the level of sophistication to static DFT or static exchange, possibly TDDFT. One should note recent developments in non-equilibrium green's function codes [162] and ADC(2) propagators [174]. Simpler treatments employing plane or coulomb waves appear more problematic [9]. Also the use of strong IR pulses either for the pump or the probe steps are within reach [175, 176, 177]. Notably a full simulation including both pump and probe pulses within a limited manifold of neutral, cation and dication states, including electron continuum and double continuum as plane waves, has been performed [175]. The treatment of nuclear motion has also received a lot of attention, although it is difficult to propagate a coherent electron-nuclear wavepacket. Besides Ehrenfest dynamics, the well-established surface-hopping method has been applied to study charge transfer following ionization to a single cationic state [178]. Multiple Spawning [179, 180] and MCTDH [181, 182, 183] appear promising for the combined task, although limited by the large number of degrees of freedom. Such studies have provided evidence that the fixed nuclei treatment is often a reasonable description in the first 10 or more fs, although very fast decoherence may occur when potential energy surfaces cross or have very different slopes [69]. In any case final charge localization is necessarily associated with nuclear dynamics. More accurate calculations, approaching a full quantum

treatment, are within reach in the smallest systems, like diatomics, which can shed light on limitations of the more viable treatments available for larger molecules [47, 48, 184].

8. – Conclusions

One of the scientific challenges of direct biological relevance is the understanding of photo-induced damage/mutation and, more generally, structural changes of our own biomolecules, including the underlying coupled electron-nuclear dynamics triggered by the interaction with high-energy photons. Attosecond science provides a valuable tool for the investigation of the role of the activated electron dynamics in the photochemistry of complex molecules and progress in this direction has been done by real-time tracing of electronic charge flow in aromatic amino acids. Advances have been also achieved in the development of new theoretical models to describe the full quantum dynamics of the molecular system. Current and future developments in attosecond technology (for instance at the new European facility ELI-ALPS) will enable the development of XUV sources providing higher photon flux (μJ-level) and higher repetition rates (hundreds kHz) paving the way to the investigation of even more complex biomolecular targets, which are typically produced in the gas phase with very low densities. All these advances will be key in disclosing the role of electron dynamics in the photochemistry of biochemically relevant molecules and to fully understand a number of ultrafast processes of fundamental importance in photochemistry and photobiology.

* * *

The authors acknowledge the support from the European Research Council under the ERC grants no. 637756 STARLIGHT, no. 227355 ELYCHE and no. 290853 XCHEM, LASERLAB- EUROPE (grant agreement no. 284464, European Commissions Seventh Framework Programme), European COST Action CM1204 XLIC, the Ministerio de Ciencia e Innovación project FIS2016-77889-R, European grants MC-ITN CORINF and MC-RG ATTOTREND 268284, UKs Science and Technology Facilities Council Laser Loan Scheme, the Engineering and Physical Sciences Research Council (grant EP/J007048/1), the Leverhulme Trust (grant RPG-2012-735), and the Northern Ireland Department of Employment and Learning.

REFERENCES

[1] L. Cederbaum, J. Zobeley, Ultrafast charge migration by electron correlation, Chemical Physics Letters 307 (3-4) (1999) 205–210. doi:10.1016/S0009-2614(99)00508-4.

[2] H. Hennig, J. Breidbach, L. S. Cederbaum, Electron Correlation as the Driving Force for Charge Transfer: Charge Migration Following Ion ization in N -Methyl Acetamide, The Journal of Physical Chemistry A 109 (3) (2005) 409–414. doi:10.1021/jp046232s.

[3] F. Remacle, R. D. Levine, An electronic time scale in chemistry., Proceedings of the National Academy of Sciences of the United States of America 103 (18) (2006) 6793–8. doi:10.1073/pnas.0601855103.

[4] J. Breidbach, L. S. Cederbaum, Migration of holes: Numerical algorithms and implementation, Journal of Chemical Physics 126 (3) (2007) 1–15. doi:10.1063/1.2428292.

[5] A. I. Kuleff, L. S. Cederbaum, Ultrafast correlation-driven electron dynamics, Journal of Physics B: Atomic, Molecular and Optical Physics 47 (12) (2014) 124002. doi:10.1088/0953-4075/47/12/124002.

[6] F. Lépine, M. Y. Ivanov, M. J. J. Vrakking, Attosecond molecular dynamcis: fact or fiction?, Nature Photonics 8 (2014) 195–204. doi:10.1038/nphoton.2014.25.

[7] Z. Li, O. Vendrell, R. Santra, Ultrafast charge transfer of a valence double hole in glycine driven exclusively by nuclear motion, Phys. Rev. Lett. 115 (2015) 143002. doi:10.1103/PhysRevLett.115.143002.

[8] F. Krausz, M. Ivanov, Attosecond Physics, Rev. Mod. Phys. 81 (1) (2009) 163–234. doi:10.1103/RevModPhys.81.163.

[9] M. Nisoli, P. Decleva, F. Calegari, A. Palacios, F. Martn, Attosecond electron dynamics in molecules, Chemical Reviews 117 (16) (2017) 10760–10825, pMID: 28488433. arXiv:https://doi.org/10.1021/acs.chemrev.6b00453, doi:10.1021/acs.chemrev.6b00453.

[10] G. Sansone, L. Poletto, M. Nisoli, High-Energy Attosecond Light Sources, Nat. Photonics 5 (11) (2011) 655–663. doi:10.1038/nphoton.2011.167.

[11] F. Calegari, G. Sansone, S. Stagira, C. Vozzi, M. Nisoli, Advances in attosecond science, J. Phys. B: At., Mol. Opt. Phys.: At., Mol. Opt. Phys. 49 (6) (2016) 062001.

[12] M. Hentschel, R. Kienberger, C. Spielmann, G. A. Reider, N. Milosevic, T. Brabec, P. Corkum, U. Heinzmann, M. Drescher, F. Krausz, Attosecond metrology, Nature 414 (2001) 509–513. doi:10.1038/35107000.

[13] E. Goulielmakis, M. Schultze, M. Hofstetter, V. S. Yakovlev, J. Gagnon, M. Uiberacker, A. L. Aquila, E. M. Gullikson, D. T. Attwood, R. Kienberger, et al., Single-cycle nonlinear optics, Science 320 (5883) (2008) 1614–1617. arXiv:http://science.sciencemag.org/content/320/5883/1614.full.pdf, doi:10.1126/science.1157846.

[14] P. B. Corkum, N. H. Burnett, M. Y. Ivanov, Subfemtosecond pulses, Opt. Lett. 19 (22) (1994) 1870–1872. doi:10.1364/OL.19.001870.

[15] I. Sola, E. Mével, L. Elouga, E. Constant, V. Strelkov, L. Poletto, P. Villoresi, E. Benedetti, J. P. Caumes, S. Stagira, et al., Controlling attosecond electron dynamics by phase-stabilized polarization gating, Nat. Phys. 2 (2006) 319–322.

[16] G. Sansone, E. Benedetti, F. Calegari, C. Vozzi, L. Avaldi, R. Flammini, L. Poletto, P. Villoresi, C. Altucci, R. Velotta, et al., Isolated single-cycle attosecond pulses, Science 314 (5798) (2006) 443–446. arXiv:http://science.sciencemag.org/content/314/5798/443.full.pdf, doi:10.1126/science.1132838.

[17] Z. Chang, Controlling attosecond pulse generation with a double optical gating, Phys. Rev. A 76 (2007) 051403. doi:10.1103/PhysRevA.76.051403.

[18] H. Mashiko, S. Gilbertson, C. Li, S. D. Khan, M. M. Shakya, E. Moon, Z. Chang, Double Optical Gating of High-Order Harmonic Generation with Carrier-Envelope Phase Stabilized Lasers, Phys. Rev. Lett. 100 (10) (2008) 103906. doi:10.1103/PhysRevLett.100.103906.

[19] X. Feng, S. Gilbertson, H. Mashiko, H. Wang, S. D. Khan, M. Chini, Y. Wu, K. Zhao, Z. Chang, Generation of isolated attosecond pulses with 20 to 28 femtosecond lasers, Phys. Rev. Lett. 103 (2009) 183901. doi:10.1103/PhysRevLett.103.183901.

[20] F. Ferrari, F. Calegari, M. Lucchini, C. Vozzi, S. Stagira, G. Sansone, M. Nisoli, High-Energy Isolated Attosecond Pulses Generated by Above-Saturation Few-Cycle Fields, Nat. Photonics 4 (12) (2010) 875–879.

[21] A. Wirth, M. T. Hassan, I. Grguraš, J. Gagnon, A. Moulet, T. T. Luu, S. Pabst, R. Santra, Z. A. Alahmed, A. M. Azzeer, et al., Synthesized light transients, Science 334 (6053) (2011) 195–200. arXiv:http://science.sciencemag.org/content/334/6053/195.full.pdf, doi:10.1126/science.1210268.

[22] M. T. Hassan, A. Wirth, I. Grguraš, A. Moulet, T. T. Luu, J. Gagnon, V. Pervak, E. Goulielmakis, Attosecond photonics: Synthesis and control of light transients, Rev. Sci. Instrum. 83 (11) (2012) 111301. doi:http://dx.doi.org/10.1063/1.4758310.

[23] M. T. Hassan, T. T. Luu, A. Moulet, O. Raskazovskaya, P. Zhokhov, M. Garg, N. Karpowicz, A. M. Zheltikov, V. Pervak, F. Krausz, et al., Optical attosecond pulses and tracking the nonlinear response of bound electrons, Nature 530 (2016) 66–70. doi:10.1038/nature16528.

[24] C. Manzoni, O. D. Mücke, G. Cirmi, S. Fang, J. Moses, S.-W. Huang, K.-H. Hong, G. Cerullo, F. X. Kërtner, Coherent pulse synthesis: towards sub-cycle optical waveforms, Laser Photonics Reviews 9 (2) (2015) 129–171. doi:10.1002/lpor.201400181.

[25] E. Goulielmakis, M. Uiberacker, R. Kienberger, A. Baltuska, V. Yakovlev, A. Scrinzi, T. Westerwalbesloh, U. Kleineberg, U. Heinzmann, M. Drescher, et al., Direct measurement of light waves, Science 305 (5688) (2004) 1267–1269. arXiv:http://science.sciencemag.org/content/305/5688/1267.full.pdf, doi:10.1126/science.1100866.

[26] T. Popmintchev, M.-C. Chen, D. Popmintchev, P. Arpin, S. Brown, S. Alisauskas, G. Andriukaitis, T. Balciunas, O. D. Mucke, A. Pugzlys, et al., Bright Coherent Ultrahigh Harmonics in the keV X-ray Regime from Mid-Infrared Femtosecond Lasers, Science 336 (6086) (2012) 1287–1291. doi:10.1126/science.1218497.

[27] U. C. Tseng T.-C., O. R. Wang Y., A. M. Tait S. L., E. D., T. M., G. J. M., L. N., K. M., S. U., N. A., L. A., W. C., H. M. A., M. F., M. N., K. K., M. R., Charge-transfer-induced structural rearrangements at both sides of organic/metal interfaces, Nature Chem. 2 (2010) 374–379. doi:10.1038/nchem.591.

[28] G. Griffini, L. Brambilla, M. Levi, M. D. Zoppo, S. Turri, Photo-degradation of a perylene-based organic luminescent solar concentrator: Molecular aspects and device implications, Solar Energy Materials and Solar Cells 111 (2013) 41 – 48. doi:https://doi.org/10.1016/j.solmat.2012.12.021.

[29] R. Boll, D. Anielski, C. Bostedt, J. D. Bozek, L. Christensen, R. Coffee, S. De, P. Decleva, S. W. Epp, B. Erk, L. Foucar, F. Krasniqi, J. Küpper, A. Rouzée, B. Rudek, A. Rudenko, S. Schorb, H. Stapelfeldt, M. Stener, S. Stern, S. Techert, S. Trippel, M. J. J. Vrakking, J. Ullrich, D. Rolles, Femtosecond photoelectron diffraction on laser-aligned molecules: Towards time-resolved imaging of molecular structure, Phys. Rev. A 88 (2013) 061402. doi:10.1103/PhysRevA.88.061402.

[30] B. Shan, Z. Chang, Dramatic extension of the high-order harmonic cutoff by using a long-wavelength driving field, Phys. Rev. A 65 (2001) 011804. doi:10.1103/PhysRevA.65.011804.

[31] T. Popmintchev, M.-C. Chen, O. Cohen, M. E. Grisham, J. J. Rocca, M. M. Murnane, H. C. Kapteyn, Extended phase matching of high harmonics driven by mid-infrared light, Opt. Lett. 33 (18) (2008) 2128–2130. doi:10.1364/OL.33.002128.

[32] P. Colosimo, G. Doumy, C. I. Blaga, J. Wheeler, C. Hauri, F. Catoire, J. Tate, R. Chirla, a. M. March, G. G. Paulus, et al., Scaling Strong-Field Interactions Towards the Classical Limit, Nat. Phys. 4 (5) (2008) 386–389. arXiv:9702041, doi:10.1038/nphys914.

[33] E. J. Takahashi, T. Kanai, K. L. Ishikawa, Y. Nabekawa, K. Midorikawa, Coherent water window x ray by phase-matched high-order harmonic generation in neutral media, Phys. Rev. Lett. 101 (2008) 253901. doi:10.1103/PhysRevLett.101.253901.

[34] C. Vozzi, F. Calegari, F. Frassetto, L. Poletto, G. Sansone, P. Villoresi, M. Nisoli, S. De Silvestri, S. Stagira, Coherent Continuum Generation Above 100 ev Driven by an Ir Parametric Source in a Two-Color Scheme, Phys. Rev. A 79 (3) (2009) 033842. doi:10.1103/PhysRevA.79.033842.

[35] A. D. Shiner, C. Trallero-Herrero, N. Kajumba, H.-C. Bandulet, D. Comtois, F. Légaré, M. Giguère, J.-C. Kieffer, P. B. Corkum, D. M. Villeneuve, Wavelength scaling of high harmonic generation efficiency, Phys. Rev. Lett. 103 (2009) 073902. doi:10.1103/PhysRevLett.103.073902.

[36] S. L. Cousin, N. Di Palo, B. Buades, S. M. Teichmann, M. Reduzzi, M. Devetta, A. Kheifets, G. Sansone, J. Biegert, Attosecond streaking in the water window: A new regime of attosecond pulse characterization, Phys. Rev. X 7 (2017) 041030. doi:10.1103/PhysRevX.7.041030.

[37] P. Tzallas, E. Skantzakis, L. A. A. Nikolopoulos, G. D. Tsakiris, D. Charalambidis, Extreme-Ultraviolet Pump-Probe Studies of One-Femtosecond-Scale Electron Dynamics, Nat. Phys. 7 (10) (2011) 781–784.

[38] P. A. Carpeggiani, P. Tzallas, A. Palacios, D. Gray, F. Martín, D. Charalambidis, Disclosing intrinsic molecular dynamics on the 1-fs scale through extreme-ultraviolet pump-probe measurements, Phys. Rev. A 89 (2014) 023420. doi:10.1103/PhysRevA.89.023420.

[39] E. J. Takahashi, P. Lan, O. D. Mücke, Y. Nabekawa, K. Midorikawa, Attosecond nonlinear optics using gigawatt-scale isolated attosecond pulses, Nat. Commun. 4 (2013) 2691.

[40] F. Calegari, C. Vozzi, M. Negro, G. Sansone, F. Frassetto, L. Poletto, P. Villoresi, M. Nisoli, S. D. Silvestri, S. Stagira, Efficient continuum generation exceeding 200 ev by intense ultrashort two-color driver, Opt. Lett. 34 (20) (2009) 3125–3127. doi:10.1364/OL.34.003125.

[41] E. J. Takahashi, P. Lan, O. D. Mücke, Y. Nabekawa, K. Midorikawa, Infrared two-color multicycle laser field synthesis for generating an intense attosecond pulse, Phys. Rev. Lett. 104 (2010) 233901. doi:10.1103/PhysRevLett.104.233901.

[42] P. Lan, E. J. Takahashi, K. Midorikawa, Optimization of infrared two-color multicycle field synthesis for intense-isolated-attosecond-pulse generation, Phys. Rev. A 82 (2010) 053413. doi:10.1103/PhysRevA.82.053413.

[43] E. Hemsing, G. Stupakov, D. Xiang, A. Zholents, Beam by design: Laser manipulation of electrons in modern accelerators, Rev. Mod. Phys. 86 (2014) 897–941. doi:10.1103/RevModPhys.86.897.

[44] I. P. S. Martin, R. Bartolini, Comparison of short pulse generation schemes for a soft x-ray free electron laser, Phys. Rev. ST Accel. Beams 14 (2011) 030702. doi:10.1103/PhysRevSTAB.14.030702.

[45] R. Bonifacio, L. De Salvo, P. Pierini, N. Piovella, C. Pellegrini, Spectrum, temporal structure, and fluctuations in a high-gain free-electron laser starting from noise, Phys. Rev. Lett. 73 (1994) 70–73. doi:10.1103/PhysRevLett.73.70.

[46] W. Helml, A. Maier, W. Schweinberger, I. Grguraš, P. Radcliffe, G. Doumy, C. Roedig, J. Gagnon, M. Messerschmidt, S. Schorb, et al., Measuring the Temporal Structure of Few-Femtosecond Free-Electron Laser X-Ray Pulses Directly in the Time Domain, Nat. Photonics 8 (12) (2014) 950–957.

[47] G. Sansone, F. Kelkensberg, J. F. Pérez-Torres, F. Morales, M. F. Kling, W. Siu, O. Ghafur, P. Johnsson, M. Swoboda, E. Benedetti, F. Ferrari, F. Lepine, J. L. Sanz-Vicario, S. Zherebtsov, I. Znakovskaya, A. L'Huillier, M. Y. Ivanov, M. Nisoli, F. Martín, M. J. J. Vrakking, Electron localization following attosecond molecular photoionization, nature 465 (7299) (2010) 763. doi:10.1038/nature09084.

[48] A. Trabattoni, M. Klinker, J. González-Vázquez, C. Liu, G. Sansone, R. Linguerri, M. Hochlaf, J. Klei, M. J. J. Vrakking, F. Martín, M. Nisoli, F. Calegari, Mapping the dissociative ionization dynamics of molecular nitrogen with attosecond time resolution, Phys. Rev. X 5 (2015) 041053. doi:10.1103/PhysRevX.5.041053.

[49] E. R. Warrick, J. E. Baekhoj, W. Cao, A. P. Fidler, F. Jensen, L. B. Madsen, S. R. Leone, D. M. Neumark, Attosecond transient absorption spectroscopy of molecular nitrogen: Vibrational coherences in the b'1 1s+u state, Chemical Physics Letters 683 (2017) 408 – 415, ahmed Zewail (1946-2016) Commemoration Issue of Chemical Physics Letters. doi:https://doi.org/10.1016/j.cplett.2017.02.013.

[50] S. Beaulieu, A. Comby, A. Clergerie, J. Caillat, D. Descamps, N. Dudovich, B. Fabre, R. Géneaux, F. Légaré, S. Petit, B. Pons, G. Porat, T. Ruchon, R. Taïeb, V. Blanchet, Y. Mairesse, Attosecond-resolved photoionization of chiral molecules, Science 358 (6368) (2017) 1288–1294. arXiv:http://science.sciencemag.org/content/358/6368/1288.full.pdf, doi:10.1126/science.aao5624.

[51] F. Kelkensberg, W. Siu, J. F. Pérez-Torres, F. Morales, G. Gademann, A. Rouzée, P. Johnsson, M. Lucchini, F. Calegari, J. L. Sanz-Vicario, F. Martín, M. J. J. Vrakking, Attosecond control in photoionization of hydrogen molecules, Phys. Rev. Lett. 107 (2011) 043002. doi:10.1103/PhysRevLett.107.043002.

[52] W. Siu, F. Kelkensberg, G. Gademann, A. Rouzée, P. Johnsson, D. Dowek, M. Lucchini, F. Calegari, U. De Giovannini, A. Rubio, R. R. Lucchese, H. Kono, F. Lépine, M. J. J.

Vrakking, Attosecond control of dissociative ionization of o_2 molecules, Phys. Rev. A 84 (2011) 063412. doi:10.1103/PhysRevA.84.063412.

[53] P. Cörlin, A. Fischer, M. Schönwald, A. Sperl, T. Mizuno, U. Thumm, T. Pfeifer, R. Moshammer, Probing calculated $o_2{}^+$ potential-energy curves with an xuv-ir pump-probe experiment, Phys. Rev. A 91 (2015) 043415. doi:10.1103/PhysRevA.91.043415.

[54] A. S. Sandhu, E. Gagnon, R. Santra, V. Sharma, W. Li, P. Ho, P. Ranitovic, C. L. Cocke, M. M. Murnane, H. C. Kapteyn, Observing the creation of electronic feshbach resonances in soft x-ray–induced o2 dissociation, Science 322 (5904) (2008) 1081–1085. arXiv:http://science.sciencemag.org/content/322/5904/1081.full.pdf, doi:10.1126/science.1164498.

[55] I. Znakovskaya, P. von den Hoff, S. Zherebtsov, A. Wirth, O. Herrwerth, M. J. J. Vrakking, R. de Vivie-Riedle, M. F. Kling, Attosecond control of electron dynamics in carbon monoxide, Phys. Rev. Lett. 103 (2009) 103002. doi:10.1103/PhysRevLett.103.103002.

[56] L. Poletto, P. Villoresi, F. Frassetto, F. Calegari, F. Ferrari, M. Lucchini, G. Sansone, M. Nisoli, Time-delay compensated monochromator for the spectral selection of extreme-ultraviolet high-order laser harmonics, Review of Scientific Instruments 80 (12) (2009) 123109. doi:10.1063/1.3273964.
URL `https://doi.org/10.1063/1.3273964`

[57] M. Eckstein, C.-H. Yang, M. Kubin, F. Frassetto, L. Poletto, H.-H. Ritze, M. J. J. Vrakking, O. Kornilov, Dynamics of n2 dissociation upon inner-valence ionization by wavelength-selected xuv pulses, The Journal of Physical Chemistry Letters 6 (3) (2015) 419–425. doi:10.1021/jz5025542.

[58] H. Wang, M. Chini, S. Chen, C.-H. Zhang, F. He, Y. Cheng, Y. Wu, U. Thumm, Z. Chang, Attosecond time-resolved autoionization of argon, Phys. Rev. Lett. 105 (2010) 143002. doi:10.1103/PhysRevLett.105.143002.

[59] W. Cao, E. R. Warrickand, D. M. Neumark, S. R. Leone, Excited-state vibronic wave-packet dynamics in h2 probed by xuv transient four-wave mixing, New J. Phys. 18 (2016) 13041.

[60] X. Wang, M. Chini, Y. Cheng, Y. Wu, X.-M. Tong, Z. Chang, Subcycle laser control and quantum interferences in attosecond photoabsorption of neon, Phys. Rev. A 87 (2013) 063413. doi:10.1103/PhysRevA.87.063413.

[61] A. R. Beck, B. Bernhardt, E. R. Warrick, M. Wu, S. Chen, M. B. Gaarde, K. J. Schafer, D. M. Neumark, S. R. Leone, Attosecond transient absorption probing of electronic superpositions of bound states in neon: detection of quantum beats, New Journal of Physics 16 (11) (2014) 113016.

[62] M. Chini, X. Wang, Y. Cheng, Y. Wu, d. Zhao, D. Telnov, S.-I. Chu, Z. Chang, Sub-cycle oscillations in virtual states brought to light, Scientific Reports 3 (2013) 1105.

[63] S. Chen, M. J. Bell, A. R. Beck, H. Mashiko, M. Wu, A. N. Pfeiffer, M. B. Gaarde, D. M. Neumark, S. R. Leone, K. J. Schafer, Light-induced states in attosecond transient absorption spectra of laser-dressed helium, Phys. Rev. A 86 (2012) 063408. doi:10.1103/PhysRevA.86.063408.

[64] C. Ott, A. Kaldun, L. Argenti, P. Raith, K. Meyer, M. Laux, Y. Zhang, A. Blättermann, S. Hagstotz, T. Ding, et al., Reconstruction and control of a time-dependent two-electron wave packet, Nature 516 (7531) (2014) 374.

[65] M. Reduzzi, W.-C. Chu, C. Feng, A. Dubrouil, J. Hummert, F. Calegari, F. Frassetto, L. Poletto, O. Kornilov, M. Nisoli, C.-D. Lin, G. Sansone, Observation of autoionization dynamics and sub-cycle quantum beating in electronic molecular wave packets, Journal of Physics B: Atomic, Molecular and Optical Physics 49 (6) (2016) 065102.

[66] M. Huppert, I. Jordan, D. Baykusheva, A. von Conta, H. J. Wörner, Attosecond delays in molecular photoionization, Phys. Rev. Lett. 117 (2016) 093001.

[67] K. Spinlove, M. Vacher, M. Bearpark, M. Robb, G. Worth, Using quantum dynamics simulations to follow the competition between charge migration and charge transfer in polyatomic molecules, Chemical Physics 482 (2017) 52 – 63, electrons and nuclei in motion - correlation and dynamics in molecules (on the occasion of the 70th birthday of Lorenz S. Cederbaum). doi:https://doi.org/10.1016/j.chemphys.2016.10.007.

[68] H. J. Woerner, C. A. Arrell, N. Banerji, A. Cannizzo, M. Chergui, A. K. Das, P. Hamm, U. Keller, P. M. Kraus, E. Liberatore, P. Lopez-Tarifa, M. Lucchini, M. Meuwly, C. Milne, J.-E. Moser, U. Rothlisberger, G. Smolentsev, J. Teuscher, J. A. van Bokhoven, O. Wenger, Charge migration and charge transfer in molecular systems, Structural Dynamics 4 (6) (2017) 061508. arXiv:https://doi.org/10.1063/1.4996505, doi:10.1063/1.4996505.

[69] M. Vacher, L. Steinberg, A. J. Jenkins, M. J. Bearpark, M. A. Robb, Electron dynamics following photoionization: Decoherence due to the nuclear-wave-packet width, Phys. Rev. A 92 (2015) 040502. doi:10.1103/PhysRevA.92.040502.

[70] M. Lara-Astiaso, D. Ayuso, I. Tavernelli, P. Decleva, A. Palacios, F. Martin, Decoherence, control and attosecond probing of XUV-induced charge migration in biomolecules. a theoretical outlook, Faraday Discuss. 194 (2016) 41–59. doi:10.1039/C6FD00074F.

[71] F. Calegari, D. Ayuso, A. Trabattoni, L. Belshaw, S. De Camillis, S. Anumula, F. Frassetto, L. Poletto, A. Palacios, P. Decleva, J. B. Greenwood, F. Martín, M. Nisoli, Ultrafast electron dynamics in phenylalanine initiated by attosecond pulses, Science 346 (6207) (2014) 336–339. arXiv:http://science.sciencemag.org/content/346/6207/336.full.pdf, doi:10.1126/science.1254061.

[72] A. I. Kuleff, N. V. Kryzhevoi, M. Pernpointner, L. S. Cederbaum, Core ionization initiates subfemtosecond charge migration in the valence shell of molecules, Phys. Rev. Lett. 117 (2016) 093002. doi:10.1103/PhysRevLett.117.093002.

[73] M. Hollstein, R. Santra, D. Pfannkuche, Correlation-driven charge migration following double ionization and attosecond transient absorption spectroscopy, Phys. Rev. A 95 (2017) 053411. doi:10.1103/PhysRevA.95.053411.

[74] L. Young, K. Ueda, M. Guehr, P. H. Bucksbaum, M. Simon, S. Mukamel, N. Rohringer, K. C. Prince, C. Masciovecchio, M. Meyer, A. Rudenko, D. Rolles, C. Bostedt, M. Fuchs, D. A. Reis, R. Santra, H. Kapteyn, M. Murnane, H. Ibrahim, F. Legare, M. Vrakking, M. Isinger, D. Kroon, M. Gisselbrecht, A. L'Huillier, H. J. Woerner, S. R. Leone, Roadmap of ultrafast x-ray atomic and molecular physics, J. Phys. B: At., Mol. Opt. Phys. 51 (3) (2018) 032003.

[75] L. Belshaw, F. Calegari, M. J. Duffy, A. Trabattoni, L. Poletto, M. Nisoli, J. B. Greenwood, Observation of ultrafast charge migration in an amino acid, The Journal of Physical Chemistry Letters 3 (24) (2012) 3751–3754, pMID: 26291106. arXiv:https://doi.org/10.1021/jz3016028, doi:10.1021/jz3016028.

[76] F. Cailliez, P. Mueller, T. Firmino, P. Pernot, A. de la Lande, Energetics of photoinduced charge migration within the tryptophan tetrad of an animal (6-4) photolyase, Journal of the American Chemical Society 138 (6) (2016) 1904–1915, pMID: 26765169. arXiv:https://doi.org/10.1021/jacs.5b10938, doi:10.1021/jacs.5b10938.

[77] K. Rottger, H. J. B. Marroux, M. P. Grubb, P. M. Coulter, H. Bohnke, A. S. Henderson, M. C. Galan, F. Temps, A. J. Orr-Ewing, G. M. Roberts, Ultraviolet absorption induces hydrogen-atom transfer in g c watson-crick dna base pairs in solution, Angewandte Chemie 127 (49) (2015) 14932–14935. doi:10.1002/ange.201506940.

[78] M. Raytchev, E. Mayer, N. Amann, H.-A. Wagenknecht, T. Fiebig, Ultrafast proton-coupled electron-transfer dynamics in pyrene-modified pyrimidine nucleosides: Model studies towards an understanding of reductive electron transport in DNA, ChemPhysChem 5 (5) (2004) 706–712. doi:10.1002/cphc.200301205.

[79] M. Lara-Astiaso, A. Palacios, P. Decleva, I. Tavernelli, F. Martn, Role of electron-nuclear coupled dynamics on charge migration induced by attosecond pulses in glycine, Chemical Physics Letters 683 (2017) 357 – 364, ahmed Zewail (1946-2016) Commemoration Issue of Chemical Physics Letters. doi:https://doi.org/10.1016/j.cplett.2017.05.008.

[80] A. H. Zewail, Femtochemistry: Atomic-scale dynamics of the chemical bond using ultrafast lasers (nobel lecture), Angewandte Chemie International Edition 39 (15) (2000) 2586–2631. doi:10.1002/1521-3773(20000804)39:15¡2586::AID-ANIE2586¿3.0.CO;2-O.

[81] I. V. Hertel, W. Radloff, Ultrafast dynamics in isolated molecules and molecular clusters, Reports on Progress in Physics 69 (6) (2006) 1897.

[82] G. S. Schlau-Cohen, J. M. Dawlaty, G. R. Fleming, Ultrafast multidimensional spectroscopy: Principles and applications to photosynthetic systems, IEEE Journal of Selected Topics in Quantum Electronics 18 (1) (2012) 283–295. doi:10.1109/JSTQE.2011.2112640.

[83] E. Romero, R. Augulis, V. I. Novoderezhkin, M. Ferretti, J. Thieme, D. Zigmantas, R. van Grondelle, Quantum coherence in photosynthesis for efficient solar-energy conversion, Nature Physics 10 (2014) 676. doi:10.1038/nphys3017.

[84] A. Nenov, J. Segarra-Marti, A. Giussani, I. Conti, I. Rivalta, E. Dumont, V. K. Jaiswal, S. F. Altavilla, S. Mukamel, M. Garavelli, Probing deactivation pathways of dna nucleobases by two-dimensional electronic spectroscopy: first principles simulations, Faraday Discuss. 177 (2015) 345–362. doi:10.1039/C4FD00175C.

[85] A. R. Beck, D. M. Neumark, S. R. Leone, Probing ultrafast dynamics with attosecond transient absorption, Chemical Physics Letters 624 (2015) 119 – 130. doi:https://doi.org/10.1016/j.cplett.2014.12.048.

[86] C. E. Crespo-Hernandez, B. Cohen, B. Kohler, Base stacking controls excited-state dynamics in dna, Nature 436 (2005) 1141. doi:10.1038/nature03933.

[87] C. T. Middleton, K. de La Harpe, C. Su, Y. K. Law, C. E. Crespo-Hernndez, B. Kohler, Dna excited-state dynamics: From single bases to the double helix, Annual Review of Physical Chemistry 60 (1) (2009) 217–239, pMID: 19012538. arXiv:https://doi.org/10.1146/annurev.physchem.59.032607.093719, doi:10.1146/annurev.physchem.59.032607.093719.

[88] D. N. Beratan, D. H. Waldeck, Hot holes break the speed limit, Nature Chemistry 8 (2016) 992. doi:10.1038/nchem.2655.

[89] N. Renaud, M. A. Harris, A. P. N. Singh, Y. A. Berlin, M. A. Ratner, M. R. Wasielewski, F. D. Lewis, F. C. Grozema, Deep-hole transfer leads to ultrafast charge migration in DNA hairpins, Nature Chemistry 8 (2016) 1015. doi:10.1038/nchem.2590.

[90] M. Barbatti, A. C. Borin, S. Ullrich, Photoinduced Processes in Nucleic Acids I, Springer International Publishing, Cham, 2015, Ch. Photoinduced Processes in Nucleic Acids, pp. 1–32. doi:10.1007/128$_2$014$_5$69.

[91] T. Gustavsson, R. Improta, D. Markovitsi, Dna/rna: Building blocks of life under UV irradiation, The Journal of Physical Chemistry Letters 1 (13) (2010) 2025–2030. arXiv:https://doi.org/10.1021/jz1004973, doi:10.1021/jz1004973.

[92] S. De Camillis, J. Miles, G. Alexander, O. Ghafur, I. D. Williams, D. Townsend, J. B. Greenwood, Ultrafast non-radiative decay of gas-phase nucleosides, Phys. Chem. Chem. Phys. 17 (2015) 23643–23650. doi:10.1039/C5CP03806E.

[93] J.-M. L. Pecourt, J. Peon, B. Kohler, Ultrafast internal conversion of electronically excited rna and dna nucleosides in water, Journal of the American Chemical Society 122 (38) (2000) 9348–9349. arXiv:https://doi.org/10.1021/ja0021520, doi:10.1021/ja0021520.

[94] C. Wan, T. Fiebig, O. Schiemann, J. K. Barton, A. H. Zewail, Femtosecond direct observation of charge transfer between bases in DNA, Proceedings of the National Academy of Sciences 97 (26) (2000) 14052–14055. arXiv:http://www.pnas.org/content/97/26/14052.full.pdf, doi:10.1073/pnas.250483297.

[95] B. Marchetti, T. N. V. Karsili, M. N. R. Ashfold, W. Domcke, A 'bottom up', ab initio computational approach to understanding fundamental photophysical processes in nitrogen containing heterocycles, DNA bases and base pairs, Phys. Chem. Chem. Phys. 18 (2016) 20007–20027. doi:10.1039/C6CP00165C.

[96] C. E. Crespo-Hernandez, L. Martinez-Fernandez, C. Rauer, C. Reichardt, S. Mai, M. Pollum, P. Marquetand, L. Gonzlez, I. Corral, Electronic and structural elements that regulate the excited-state dynamics in purine nucleobase derivatives, J. Am. Chem. Soc. 137 (13) (2015) 4368–4381, pMID: 25763596. arXiv:https://doi.org/10.1021/ja512536c, doi:10.1021/ja512536c.

[97] V. G. Stavros, J. R. Verlet, Gas-phase femtosecond particle spectroscopy: A bottom-up approach to nucleotide dynamics, Annual Review of Physical Chemistry 67 (1) (2016) 211–232, pMID: 26980306. arXiv:https://doi.org/10.1146/annurev-physchem-040215-112428, doi:10.1146/annurev-physchem-040215-112428.

[98] I. Conti, A. Nenov, S. Hfinger, S. F. Altavilla, I. Rivalta, E. Dumont, G. Orlandi, M. Garavelli, Excited state evolution of DNA stacked adenines resolved at the CASPT2//CASSCF/amber level: from the bright to the excimer state and back, Phys. Chem. Chem. Phys. 17 (11) (2015) 7291–7302. doi:10.1039/c4cp05546b.

[99] E. P. Mansson, S. De Camillis, M. C. Castrovilli, M. Galli, M. Nisoli, F. Calegari, J. B. Greenwood, Ultrafast dynamics in the dna building blocks thymidine and thymine initiated by ionizing radiation, Phys. Chem. Chem. Phys. 19 (2017) 19815–19821. doi:10.1039/C7CP02803B.

[100] C. Hernández-García, T. Popmintchev, M. M. Murnane, H. C. Kapteyn, L. Plaja, A. Becker, A. Jaron-Becker, Isolated broadband attosecond pulse generation with near- and mid-infrared driver pulses via time-gated phase matching, Opt. Express 25 (10) (2017) 11855–11866. doi:10.1364/OE.25.011855.
URL http://www.opticsexpress.org/abstract.cfm?URI=oe-25-10-11855

[101] W. Helml, I. Grgura?, P. N. Jurani?, S. Dsterer, T. Mazza, A. R. Maier, N. Hartmann, M. Ilchen, G. Hartmann, L. Patthey, C. Callegari, J. T. Costello, M. Meyer, R. N. Coffee, A. L. Cavalieri, R. Kienberger, Ultrashort free-electron laser x-ray pulses, Applied Sciences 7 (9). doi:10.3390/app7090915.
URL http://www.mdpi.com/2076-3417/7/9/915

[102] L. Feng, H. Liu, Y. Li, W. Li, Generation of high-intensity kev single-attosecond pulse using multi-cycle spatial inhomogeneous mid-infrared field, J. Opt. Soc. Am. B 35 (5) (2018) A84–A92. doi:10.1364/JOSAB.35.000A84.
URL http://josab.osa.org/abstract.cfm?URI=josab-35-5-A84

[103] X. Ren, J. Li, Y. Yin, K. Zhao, A. Chew, Y. Wang, S. Hu, Y. Cheng, E. Cunningham, Y. Wu, M. Chini, Z. Chang, Attosecond light sources in the water window, Journal of Optics 20 (2) (2018) 023001.
URL http://stacks.iop.org/2040-8986/20/i=2/a=023001

[104] Z.-H. Loh, S. R. Leone, Capturing ultrafast quantum dynamics with femtosecond and attosecond x-ray core-level absorption spectroscopy, The Journal of Physical Chemistry Letters 4 (2) (2013) 292–302. doi:10.1021/jz301910n.

[105] M. H. Elkins, H. L. Williams, D. M. Neumark, Isotope effect on hydrated electron relaxation dynamics studied with time-resolved liquid jet photoelectron spectroscopy, The Journal of Chemical Physics 144 (18) (2016) 184503. doi:10.1063/1.4948546.

[106] C. A. Arrell, J. Ojeda, M. Sabbar, W. A. Okell, T. Witting, T. Siegel, Z. Diveki, S. Hutchinson, L. Gallmann, U. Keller, F. van Mourik, R. T. Chapman, C. Cacho, N. Rodrigues, I. C. Turcu, J. W. Tisch, E. Springate, J. P. Marangos, M. Chergui, A simple electron time-of-flight spectrometer for ultrafast vacuum ultraviolet photoelectron spectroscopy of liquid solutions, Review of Scientific Instruments 85 (10) (2014) 103117. doi:10.1063/1.4899062.

[107] I. Jordan, A. Jain, T. Gaumnitz, J. Ma, H. J. Wrner, Photoelectron spectrometer for liquid and gas-phase attosecond spectroscopy with field-free and magnetic bottle operation modes, Review of Scientific Instruments 89 (5) (2018) 053103. doi:10.1063/1.5011657.

[108] V. Conti Nibali, M. Havenith, New insights into the role of water in biological function: Studying solvated biomolecules using terahertz absorption spectroscopy in conjunction with molecular dynamics simulations, Journal of the American Chemical Society 136 (37) (2014) 12800–12807. doi:10.1021/ja504441h.

[109] O. Dopfer, M. Fujii, Probing solvation dynamics around aromatic and biological molecules at the single-molecular level, Chemical Reviews 116 (9) (2016) 5432–5463. doi:10.1021/acs.chemrev.5b00610.

[110] J. B. Greenwood, J. Miles, S. D. Camillis, P. Mulholland, L. Zhang, M. A. Parkes, H. C. Hailes, H. H. Fielding, Resonantly enhanced multiphoton ionization spectrum of the neutral green fluorescent protein chromophore, The Journal of Physical Chemistry Letters 5 (20) (2014) 3588–3592, pMID: 26278614. arXiv:https://doi.org/10.1021/jz5019256, doi:10.1021/jz5019256.

[111] K. Tanaka, The origin of macromolecule ionization by laser irradiation (nobel lecture), Angewandte Chemie International Edition 42 (33) (2003) 3860–3870. doi:10.1002/anie.200300585.

[112] J. B. Fenn, Electrospray wings for molecular elephants (nobel lecture), Angewandte Chemie International Edition 42 (33) (2003) 3871–3894. doi:10.1002/anie.200300605.

[113] G. Reitsma, O. Gonzalez-Magana, O. Versolato, M. Door, R. Hoekstra, E. Suraud, B. Fischer, N. Camus, M. Kremer, R. Moshammer, T. Schlatholter, Femtosecond laser induced ionization and dissociation of gas-phase protonated leucine enkephalin, International Journal of Mass Spectrometry 365-366 (2014) 365 – 371, special issue: Tilmann Maerk. doi:https://doi.org/10.1016/j.ijms.2014.01.004.

[114] C. R. S. Mooney, D. A. Horke, A. S. Chatterley, A. Simperler, H. H. Fielding, J. R. R. Verlet, Taking the green fluorescence out of the protein: dynamics of the isolated gfp chromophore anion, Chem. Sci. 4 (2013) 921–927. doi:10.1039/C2SC21737F.

[115] G. Feraud, C. Dedonder, C. Jouvet, Y. Inokuchi, T. Haino, R. Sekiya, T. Ebata, Development of ultraviolet-ultraviolet hole-burning spectroscopy for cold gas-phase ions, The Journal of Physical Chemistry Letters 5 (7) (2014) 1236–1240, pMID: 26274477. arXiv:https://doi.org/10.1021/jz500478w, doi:10.1021/jz500478w.

[116] A. S. Chatterley, C. W. West, V. G. Stavros, J. R. R. Verlet, Time-resolved photoelectron imaging of the isolated deprotonated nucleotides, Chem. Sci. 5 (2014) 3963–3975. doi:10.1039/C4SC01493F.

[117] N. R. Hutzler, H.-I. Lu, J. M. Doyle, The buffer gas beam: An intense, cold, and slow source for atoms and molecules, Chemical Reviews 112 (9) (2012) 4803–4827, pMID: 22571401. arXiv:https://doi.org/10.1021/cr200362u, doi:10.1021/cr200362u.

[118] K. Tanaka, H. Waki, Y. Ido, S. Akita, Y. Yoshida, T. Yoshida, T. Matsuo, Protein and polymer analyses up to m/z 100 000 by laser ionization time-of-flight mass spectrometry, Rapid Communications in Mass Spectrometry 2 (8) (1988) 151–153. doi:10.1002/rcm.1290020802.

[119] M. Taherkhani, M. Riese, M. BenYezzar, K. Moeller-Dethlefs, A novel experimental system of high stability and lifetime for the laser-desorption of biomolecules, Review of Scientific Instruments 81 (6) (2010) 063101. arXiv:https://doi.org/10.1063/1.3373977, doi:10.1063/1.3373977.

[120] H. Saigusa, A. Tomioka, T. Katayama, E. Iwase, A matrix-free laser desorption method for production of nucleobase clusters and their hydrates, Chemical Physics Letters 418 (1) (2006) 119 – 125. doi:https://doi.org/10.1016/j.cplett.2005.10.086.

[121] J. Wei, J. M. Buriak, G. Siuzdak, Desorption-ionization mass spectrometry on porous silicon, Nature 399 (1999) 243. doi:10.1038/20400.

[122] R. Arakawa, H. Kawasaki, Functionalized nanoparticles and nanostructured surfaces for surface-assisted laser desorption/ionization mass spectrometry, Analytical Sciences 26 (12) (2010) 1229–1240. doi:10.2116/analsci.26.1229.

[123] D. A. Allwood, R. W. Dreyfus, I. K. Perera, P. E. Dyer, Uv optical absorption of matrices used for matrix-assisted laser desorption/ionization, Rapid Communications in Mass Spectrometry 10 (13) (1996) 1575–1578. doi:10.1002/(SICI)1097-0231(199610)10:13¡1575::AID-RCM658¿3.0.CO;2-C.

[124] T. L. Merrigan, C. A. Hunniford, D. J. Timson, T. Morrow, M. Catney, R. W. McCullough, Formation of gas phase macromolecular targets by laser desorption from surfaces, Journal of Physics: Conference Series 101 (1) (2008) 012016.

[125] R. B. Hall, Pulsed-laser-induced desorption studies of the kinetics of surface reactions, The Journal of Physical Chemistry 91 (5) (1987) 1007–1015. arXiv:https://doi.org/10.1021/j100289a003, doi:10.1021/j100289a003.

[126] R. J. Levis, Laser desorption and ejection of biomolecules from the condensed phase into the gas phase, Annual Review of Physical Chemistry 45 (1) (1994) 483–518, pMID: 7811355. arXiv:https://doi.org/10.1146/annurev.pc.45.100194.002411, doi:10.1146/annurev.pc.45.100194.002411.

[127] D. H. Levy, The spectroscopy of very cold gases, Science 214 (4518) (1981) 263–269.

[128] J. R. Cable, M. J. Tubergen, D. H. Levy, Laser desorption molecular beam spectroscopy: the electronic spectra of tryptophan peptides in the gas phase, Journal of the American Chemical Society 109 (20) (1987) 6198–6199. arXiv:https://doi.org/10.1021/ja00254a057, doi:10.1021/ja00254a057.

[129] U. Boesl, J. Grotemeyer, K. Walter, E. Schlag, A high-resolution time-of-flight mass spectrometer with laser desorption and a laser ionization source, Instrumentation Science

& Technology 16 (1) (1987) 151–171. arXiv:https://doi.org/10.1080/10739148708543633, doi:10.1080/10739148708543633.

[130] L. Li, D. M. Lubman, Pulsed laser desorption method for volatilizing thermally labile molecules for supersonic jet spectroscopy, Review of Scientific Instruments 59 (4) (1988) 557–561. arXiv:https://doi.org/10.1063/1.1139832, doi:10.1063/1.1139832.

[131] P. Arrowsmith, M. S. de Vries, H. E. Hunziker, H. R. Wendt, Laser desorption in front of a free jet nozzle: Distribution of desorbed material in the gas expansion, AIP Conference Proceedings 172 (1) (1988) 770–772. arXiv:http://aip.scitation.org/doi/pdf/10.1063/1.37480, doi:10.1063/1.37480.

[132] G. Meijer, M. S. de Vries, H. E. Hunziker, H. R. Wendt, Laser desorption jet-cooling of organic molecules, Applied Physics B 51 (6) (1990) 395–403. doi:10.1007/BF00329101.

[133] N. Teschmit, K. Dlugolecki, D. Gusa, I. Rubinsky, D. A. Horke, J. Kuepper, Characterizing and optimizing a laser-desorption molecular beam source, The Journal of Chemical Physics 147 (14) (2017) 144204. arXiv:https://doi.org/10.1063/1.4991639, doi:10.1063/1.4991639, arXiv:1706.04083v2.

[134] B. Lindner, U. Seydel, Laser desorption mass spectrometry of nonvolatiles under shock wave conditions, Analytical Chemistry 57 (4) (1985) 895–899. arXiv:https://doi.org/10.1021/ac00281a027, doi:10.1021/ac00281a027.

[135] A. V. Zinovev, I. V. Veryovkin, J. F. Moore, M. J. Pellin, Laser-driven acoustic desorption of organic molecules from back-irradiated solid foils, Analytical Chemistry 79 (21) (2007) 8232–8241, pMID: 17914890. arXiv:https://doi.org/10.1021/ac070584o, doi:10.1021/ac070584o.

[136] U. Sezer, L. Woerner, J. Horak, L. Felix, J. Tuxen, C. Gotz, A. Vaziri, M. Mayor, M. Arndt, Laser-induced acoustic desorption of natural and functionalized biochromophores, Analytical Chemistry 87 (11) (2015) 5614–5619. arXiv:https://doi.org/10.1021/acs.analchem.5b00601, doi:10.1021/acs.analchem.5b00601.

[137] J. Perez, L. E. Ramirez-Arizmendi, C. J. Petzold, L. P. Guler, E. D. Nelson, H. I. Kenttamaa, Laser-induced acoustic desorption/chemical ionization in fourier-transform ion cyclotron resonance mass spectrometry, International Journal of Mass Spectrometry 198 (3) (2000) 173 – 188. doi:https://doi.org/10.1016/S1387-3806(00)00181-0.

[138] R. C. Shea, C. J. Petzold, J. L. Campbell, S. Li, D. J. Aaserud, H. I. Kenttamaa, Characterization of laser-induced acoustic desorption coupled with a fourier transform ion cyclotron resonance mass spectrometer, Analytical Chemistry 78 (17) (2006) 6133–6139, pMID: 16944895. arXiv:https://doi.org/10.1021/ac0602827, doi:10.1021/ac0602827.

[139] R. C. Shea, S. C. Habicht, W. E. Vaughn, H. I. Kenttamaa, Design and characterization of a high-power laser-induced acoustic desorption probe coupled with a fourier transform ion cyclotron resonance mass spectrometer, Analytical Chemistry 79 (7) (2007) 2688–2694, pMID: 17319645. arXiv:https://doi.org/10.1021/ac061597p, doi:10.1021/ac061597p.

[140] L. Nyadong, A. M. McKenna, C. L. Hendrickson, R. P. Rodgers, A. G. Marshall, Atmospheric pressure laser-induced acoustic desorption chemical ionization fourier transform ion cyclotron resonance mass spectrometry for the analysis of complex mixtures, Analytical Chemistry 83 (5) (2011) 1616–1623, pMID: 21306132. arXiv:https://doi.org/10.1021/ac102543s, doi:10.1021/ac102543s.

[141] C. R. Calvert, L. Belshaw, M. J. Duffy, O. Kelly, R. B. King, A. G. Smyth, T. J. Kelly, J. T. Costello, D. J. Timson, W. A. Bryan, T. Kierspel, P. Rice, I. C. E. Turcu, C. M. Cacho, E. Springate, I. D. Williams, J. B. Greenwood, Liad-fs scheme for studies of ultrafast laser interactions with gas phase biomolecules, Phys. Chem. Chem. Phys. 14 (2012) 6289–6297. doi:10.1039/C2CP23840C.

[142] M. J. Duffy, O. Kelly, C. R. Calvert, R. B. King, L. Belshaw, T. J. Kelly, J. T. Costello, D. J. Timson, W. A. Bryan, T. Kierspel, I. C. E. Turcu, C. M. Cacho, E. Springate, I. D. Williams, J. B. Greenwood, Fragmentation of neutral amino acids and small peptides by intense, femtosecond laser pulses, Journal of The American Society for Mass Spectrometry 24 (9) (2013) 1366–1375. doi:10.1007/s13361-013-0653-6.

[143] Z. Huang, T. Ossenbrggen, I. Rubinsky, M. Schust, D. A. Horke, J. Kpper, Development and characterization of a laser-induced acoustic desorption source, arXiv:1710.06684 (10 2017). doi:arXiv:1710.06684.

[144] J.-C. Poully, J. Miles, S. De Camillis, A. Cassimi, J. B. Greenwood, Proton irradiation of dna nucleosides in the gas phase, Phys. Chem. Chem. Phys. 17 (2015) 7172–7180. doi:10.1039/C4CP05303F.

[145] A. Zinovev, I. Veryovkin, M. Pellin, Molecular desorption by laser driven acoustic waves: Analytical applications and physical mechanisms, in: M. G. Beghi (Ed.), Acoustic Waves - From Microdevices to Helioseismology, InTech (Rijeka, Croatia), 2011, Ch. 16, p. 343. doi:ISBN 978-953-307-572-3.

[146] F. Calegari, D. Ayuso, A. Trabattoni, L. Belshaw, S. D. Camillis, F. Frassetto, L. Poletto, A. Palacios, P. Decleva, J. B. Greenwood, F. Martn, M. Nisoli, Ultrafast charge dynamics in an amino acid induced by attosecond pulses, IEEE Journal of Selected Topics in Quantum Electronics 21 (5) (2015) 8700512. doi:10.1109/JSTQE.2015.2419218.

[147] B. Banstola, K. K. Murray, Pulsed valve matrix-assisted ionization, Analyst 142 (2017) 1672–1675. doi:10.1039/C7AN00489C.

[148] B. Hopp, T. Smausz, Z. Antal, N. Kresz, Z. Bor, D. Chrisey, Absorbing film assisted laser induced forward transfer of fungi (trichoderma conidia), Journal of Applied Physics 96 (6) (2004) 3478–3481. arXiv:https://doi.org/10.1063/1.1782275, doi:10.1063/1.1782275.

[149] A. V. Bulgakov, N. Goodfriend, O. Nerushev, N. M. Bulgakova, S. V. Starinskiy, Y. G. Shukhov, E. E. B. Campbell, Laser-induced transfer of nanoparticles for gas-phase analysis, J. Opt. Soc. Am. B 31 (11) (2014) C15–C21. doi:10.1364/JOSAB.31.000C15.

[150] N. T. Goodfriend, S. V. Starinskiy, O. A. Nerushev, N. M. Bulgakova, A. V. Bulgakov, E. E. B. Campbell, Laser pulse duration dependence of blister formation on back-radiated Ti thin films for BB-LIFT, Applied Physics A 122 (3) (2016) 154. doi:10.1007/s00339-016-9666-x.

[151] J. Breidbach, L. S. Cederbaum, Universal attosecond response to the removal of an electron, Phys. Rev. Lett. 94 (2005) 033901. doi:10.1103/PhysRevLett.94.033901.

[152] M. Stener, A. Lisini, P. Decleva, Accurate local density photoionization cross sections by lcao stieltjes imaging approach, Int. J. Quant. Chem. 53 (2) (1995) 229–244. doi:10.1002/qua.560530208.

[153] M. Stener, P. Decleva, Time-dependent density functional calculations of molecular photoionization cross sections: N_2 and ph_3, J. Chem. Phys. 112 (24) (2000) 10871–10879. doi:10.1063/1.481755.

[154] G. F. D. Toffoli, M. Stener, P. Decleva, Convergence of the multicenter b-spline dft approach for the continuum, Chem. Phys. 276 (1) (2002) 25 – 43. doi:http://dx.doi.org/10.1016/S0301-0104(01)00549-3.

[155] M. Stener, G. Fronzoni, P. Decleva, Time-dependent density-functional theory for molecular photoionization with noniterative algorithm and multicenter b-spline basis set: Cs2 and c6h6 case studies, J. Chem. Phys. 122 (23) (2005) 234301. doi:http://dx.doi.org/10.1063/1.1937367.

[156] S. E. Canton, E. Plesiat, J. D. Bozek, B. S. Rude, P. Decleva, F. Martin, Direct observation of Young's double-slit interferences in vibrationally resolved photoionization of diatomic molecules, Proceedings of the National Academy of Sciences 108 (18) (2011) 7302–7306. doi:10.1073/pnas.1018534108.

[157] E. Kukk, D. Ayuso, T. D. Thomas, P. Decleva, M. Patanen, L. Argenti, E. Plésiat, A. Palacios, K. Kooser, O. Travnikova, S. Mondal, M. Kimura, K. Sakai, C. Miron, F. Martín, K. Ueda, Effects of molecular potential and geometry on atomic core-level photoemission over an extended energy range: The case study of the CO molecule, Phys. Rev. A 88 (3) (2013) 033412. doi:10.1103/PhysRevA.88.033412.

[158] K. Ueda, C. Miron, E. Plésiat, L. Argenti, M. Patanen, K. Kooser, D. Ayuso, S. Mondal, M. Kimura, K. Sakai, O. Travnikova, A. Palacios, P. Decleva, E. Kukk, F. Martín, Intramolecular photoelectron diffraction in the gas phase., J. Chem. Phys. 139 (12) (2013) 124306. doi:10.1063/1.4820814.

[159] D. Ayuso, M. Kimura, K. Kooser, M. Patanen, E. Plésiat, L. Argenti, S. Mondal, O. Travnikova, K. Sakai, A. Palacios, E. Kukk, P. Decleva, K. Ueda, F. Martín, C. Miron, Vibrationally Resolved B 1s Photoionization Cross Section of BF 3, J. Phys. Chem. A 119 (23) (2015) 5971–5978. doi:10.1021/jp511416h.

[160] Cpmd, copyright ibm corp 1990-2015, copyright mpi für festkörperforschung stuttgart 1997-2001, http://www.cpmd.org/ (2014).

[161] D. Mendive-Tapia, M. Vacher, M. J. Bearpark, M. A. Robb, Coupled electron-nuclear dynamics: Charge migration and charge transfer initiated near a conical intersection, The Journal of Chemical Physics 139 (4) (2013) 044110. arXiv:https://doi.org/10.1063/1.4815914, doi:10.1063/1.4815914.

[162] E. Perfetto, D. Sangalli, A. Marini, G. Stefanucci, Ultrafast charge migration in xuv photoexcited phenylalanine: A first-principles study based on real-time nonequilibrium green's functions, The Journal of Physical Chemistry Letters 0 (0) (0) 1353–1358, pMID: 29494772. doi:10.1021/acs.jpclett.8b00025.

[163] C. F. Fischer, M. Idrees, Spline methods for resonances in photoionisation cross sections, Journal of Physics B: Atomic, Molecular and Optical Physics 23 (4) (1990) 679.

[164] H. Bachau, E. Cormier, P. Decleva, J. E. Hansen, F. Martín, Applications of b-splines in atomic and molecular physics, Rep. Prog. Phys. 64 (12) (2001) 1815.

[165] T. F. Miller III, D. C. Clary, Quantum free energies of the conformers of glycine on an ab initio potential energy surface, Phys. Chem. Chem. Phys. 6 (10) (2004) 2563–2571.

[166] N. Troullier, J. L. Martins, Efficient pseudopotentials for plane-wave calculations, Phys. Rev. B 43 (1991) 1993–2006. doi:10.1103/PhysRevB.43.1993.

[167] L. Kleinman, D. M. Bylander, Efficacious form for model pseudopotentials, Phys. Rev. Lett. 48 (1982) 1425–1428.

[168] B. F. E. Curchod, U. Rothlisberger, I. Tavernelli, Trajectory-based nonadiabatic dynamics with time-dependent density functional theory, ChemPhysChem 14 (7) (2013) 1314–1340. doi:10.1002/cphc.201200941.

[169] M. Vacher, D. Mendive-Tapia, M. J. Bearpark, M. A. Robb, Electron dynamics upon ionization: Control of the timescale through chemical substitution and effect of nuclear motion, J. Chem. Phys. 142 (9) (2015) 094105. doi:http://dx.doi.org/10.1063/1.4913515.

[170] S. Lünnemann, A. I. Kuleff, L. S. Cederbaum, Ultrafast charge migration in 2-phenylethyl-N,N-dimethylamine, Chemical Physics Letters 450 (4-6) (2008) 232–235. doi:10.1016/j.cplett.2007.11.031.

[171] A. I. Kuleff, L. S. Cederbaum, Charge migration in different conformers of glycine: The role of nuclear geometry, Chemical Physics 338 (2-3) (2007) 320–328. doi:10.1016/j.chemphys.2007.04.012.

[172] M. Vacher, M. Bearpark, M. Robb, Communication: Oscillating charge migration between lone pairs persists without significant interaction with nuclear motion in the glycine and gly-gly-nh-ch3 radical cations, J. Chem. Phys. 140. doi:10.1063/1.4879516.

[173] V. Despré, A. Marciniak, V. Loriot, M. C. E. Galbraith, A. Rouzée, M. J. J. Vrakking, F. Lépine, A. I. Kuleff, Attosecond hole migration in benzene molecules surviving nuclear motion, J. Phys. Chem. Lett 6 (3) (2015) 426–431. doi:10.1021/jz502493j.

[174] M. Ruberti, P. Decleva, V. Averbukh, Multi-channel dynamics in high harmonic generation of aligned co2: ab initio analysis with time-dependent b-spline algebraic diagrammatic construction, Phys. Chem. Chem. Phys. 20 (2018) 8311–8325. doi:10.1039/C7CP07849H.
URL http://dx.doi.org/10.1039/C7CP07849H

[175] B. Mignolet, R. D. Levine, F. Remacle, Charge migration in the bifunctional PENNA cation induced and probed by ultrafast ionization: a dynamical study, Journal of Physics B: Atomic, Molecular and Optical Physics 47 (2014) 124011. doi:10.1088/0953-4075/47/12/124011.

[176] A. E. Boguslavskiy, J. Mikosch, A. Gijsbertsen, M. Spanner, S. Patchkovskii, N. Gador, M. J. J. Vrakking, A. Stolow, The multielectron ionization dynamics underlying attosecond strong-field spectroscopies, Science 335 (6074) (2012) 1336–1340. arXiv:http://science.sciencemag.org/content/335/6074/1336.full.pdf, doi:10.1126/science.1212896.
URL http://science.sciencemag.org/content/335/6074/1336

[177] S. Petretti, Y. V. Vanne, A. Saenz, A. Castro, P. Decleva, Alignment-dependent ionization of $\mathbf{n}_2$, $\mathbf{o}_2$, and co_2 in intense laser fields, Phys. Rev. Lett. 104 (2010) 223001. doi:10.1103/PhysRevLett.104.223001.
URL https://link.aps.org/doi/10.1103/PhysRevLett.104.223001

[178] S. Sun, B. Mignolet, L. Fan, W. Li, R. D. Levine, F. Remacle, Nuclear motion driven ultrafast photodissociative charge transfer of the penna cation: An experimental and computational study, The Journal of Physical Chemistry A 121 (7) (2017) 1442–1447. doi:10.1021/acs.jpca.6b12310.

[179] B. Mignolet, B. F. E. Curchod, T. J. Martnez, Communication: Xfaimsexternal field ab initio multiple spawning for electron-nuclear dynamics triggered by short laser pulses, The Journal of Chemical Physics 145 (19) (2016) 191104. doi:10.1063/1.4967761.

[180] B. Mignolet, B. F. E. Curchod, A walk through the approximations of ab initio multiple spawning, The Journal of Chemical Physics 148 (13) (2018) 134110. doi:10.1063/1.5022877.

[181] M. Beck, A. Jackle, G. Worth, H.-D. Meyer, The multiconfiguration time-dependent hartree (mctdh) method: a highly efficient algorithm for propagating wavepackets, Physics Reports 324 (1) (2000) 1 – 105. doi:https://doi.org/10.1016/S0370-1573(99)00047-2.
URL http://www.sciencedirect.com/science/article/pii/S0370157399000472

[182] C. Arnold, O. Vendrell, R. Santra, Electronic decoherence following photoionization: Full quantum-dynamical treatment of the influence of nuclear motion, Phys. Rev. A 95 (2017) 033425. doi:10.1103/PhysRevA.95.033425.
URL https://link.aps.org/doi/10.1103/PhysRevA.95.033425

[183] C. Arnold, O. Vendrell, R. Welsch, R. Santra, Control of nuclear dynamics through conical intersections and electronic coherences, Phys. Rev. Lett. 120 (2018) 123001. doi:10.1103/PhysRevLett.120.123001.
URL https://link.aps.org/doi/10.1103/PhysRevLett.120.123001

[184] K. G. Komarova, F. Remacle, R. Levine, On the fly quantum dynamics of electronic and nuclear wave packets, Chemical Physics Letters 699 (2018) 155 – 161. doi:https://doi.org/10.1016/j.cplett.2018.03.050.
URL http://www.sciencedirect.com/science/article/pii/S0009261418302343